The impact of mechanochemical activation on the physicochemical properties and pozzolanic reactivity of kaolinite, muscovite and montmorillonite

Vahiddin Alperen Baki [a], Xinyuan Ke [a,*], Andrew Heath [a], Juliana Calabria-Holley [a], Cemalettin Terzi [b], Murat Sirin [c]

[a] Department of Architecture and Civil Engineering, University of Bath, United Kingdom
[b] Department of Architecture and Civil Engineering, Recep Tayyip Erdogan University, Turkiye
[c] Central Research Laboratory, Recep Tayyip Erdogan University, Turkiye

ABSTRACT

Partially replacing cement clinkers with activated clays is one of the most promising routes to decarbonise the cement industry and tackle the climate change crisis. This study systematically investigated the impact of mechanochemical activation on the physicochemical properties of kaolinite, muscovite and montmorillonite clays, including particle size distributions, morphologies, bulk and surface chemical structures. The results suggest that mechanochemical activation treatment is particularly efficient for improving the pozzolanic activity of 2:1 clays (i.e. muscovite and montmorillonite), which are difficult to effectively activate through thermal treatments and therefore not previously been extensively used as supplementary cementitious materials (SCMs). In addition to dehydroxylation and amorphisation, mechanochemical milling also leads to surface aluminium enrichment and reduction in binding energies of both Si and Al elements, all contributing to the enhanced pozzolanic reactivity. The outcome from this study represents a step-change in scientific knowledge and extends frontiers of developing new SCMs from sustainable resources.

1. Introduction

Portland cement, one of the most widely used construction materials, contributes to around 7 % of the global anthropogenic carbon emissions and has been consumed around 2 Gt/year worldwide due to construction activities [1–4]. One of the most common routes to decarbonise Portland cement-based materials is to replace cement clinker with supplementary cementitious materials (SCMs), such as fly ash, blast furnace slag (GGBS), silica fume, calcined clays and natural pozzolans [1]. However, even though industrial by-products such as fly ash and GGBFS have demonstrated excellent performances as SCMs, their availabilities are expected to decrease in the coming decades due to the closing-down of the coal-fire power plants and transition of the steel-making industries [5,6]. Calcined clays and processed natural minerals have emerged as the most promising SCMs alternatives, especially calcined clays, with satisfactory pozzolanic properties and relatively low environmental impacts (low to medium calcination temperature and no direct CO₂ release) [7,8].

The activation treatment processes of clay minerals, i.e. thermal treatment, mechanical treatment, and chemical treatment, can alter their original crystalline structure and improve their reactivities as SCMs [7,9,10]. As one of the most commonly used activation methods, the thermal treatment of clays and other minerals can destroy their original crystalline structure and transform into disordered phases [7]. Dehydroxylation and decarbonation reactions often take place during this process [11,12]. These thermal activation processes increase the reactivity of the treated clays and minerals as SCMs mainly by improving the dissolution kinetics of Al and Si elements under $Ca(OH)_2$ saturated conditions [7,13,14]. However, not all clays and minerals can be effectively activated via the thermal process [7]. Illite and some smectite type minerals (e.g. montmorillonite) show minimal reactivity improvement after thermal activation. The limited reactivity of these thermally treated clays can be attributed to the layered structures that remained stable event after complete dehydroxylation, with the Al groups trapped between the silicate tetrahedrals [7,15]. Some minerals, such as smectite clays (e.g. illite and mica), might require relatively

high-temperature thermal treatment, i.e., above 900 °C, which in turn might lead to considerable amount of CO_2 emissions [9,16,17].

In recent years, the mechanochemical activation route is starting to gain increasing interest within both the academic research community and the industry as an alternative clean activation route to the thermal treatment [9,18,19]. The mechanochemical activation process is defined as using mechanical energy to trigger chemical and physicochemical transformations in materials [20]. Mechanochemical transformation is stimulated with grinding and co-grinding energy supplied by milling, typically with a digitally controlled planetary milling at room temperature [21–24]. These processes can lead to changes of the reactivity or physicochemical properties of solid by shearing, compression, extension, bending, and impact [25]. Modified surface morphologies of the treated materials, such as increasing surface area and creating defects in crystal structures, can also be achieved during the mechanochemical processes [9,18]. The initial mechanochemical activation stage leads to decreased crystallinity (amorphisation) which is controlled by the rate of stress and energy transfer efficiency during the milling process [26]. The rate of stress and energy transfer efficiency are controlled by the ball to powder mass ratio and jar rotation speed, which affects kinetic energy and can be altered to provide a more efficient milling process [27]. Urakaev and Boldyrev reported that the degree of mechanochemical transformation is generally a function of the number of milling balls, the ball size to the diameter of the jar, milling ball properties, rotational frequency, and time [28]. The mechanochemical processes are simple and environmentally friendly alternatives to the thermal activation process and can potentially reduce the energy requirement by 50 % to 90 % [19] compared with thermal activation. It also has the potential to achieve matching cost-effectiveness as the conventional thermal activation process with optimised logistic plans, i.e., mechanochemical activation process offers the possibility to be carried out at the mining site and therefore significantly reduce the cost of transportation and thus reducing the cost of the final products [29].

Kaolin is one of the most commonly studied minerals for mechanochemical activation [11,18,30,31]. During the initial mechanochemical milling process, the crystallinity of the kaolin mineral decreases while the specific surface area increases. Further mechanochemical milling leads to complete delamination of the kaolin through dehydroxylation reaction which also increases the surface absorbed water [9,18,31]. The specific surface area increases to a maximal value and decreases at extended duration of milling due to agglomeration of the amorphised particles [18,32]. The chemical and physical changes induced by the mechanochemical activation process enhance the pozzolanic reactivity of the treated kaolin [32,33], with potential to achieve higher pozzolanic reactivity comparing to thermal treatment at the same cement replacement level [18]. Similar activation effects have also been reported by very recent studies for muscovite and other natural clays where mechanochemical activation leads to significant increase of dissolution ratio and pozzolanic activity at optimised activation conditions comparing to these clay minerals in their original form [32,34,35]. However, despite the recent progress in applying mechanochemical treatment as an effective methods to activate clay minerals for using as SCMs, the fundamental understanding of the complex physicochemical reactions occurring during the activation process, from atomic to mesoscale, is still limited. The effects of mechanochemical reactions on the surface modification of these minerals also remain largely unclear. Besides, the use of 2:1 clays could have benefits above those observed with kaolinite (1:1 mineral) due to the additional silica layer potentially promoting additional calcium silicate hydrate formation, however, thermal activation has been proven to only have limited activation effect on these minerals [7,36]. Therefore, it is particularly valuable to explore the use of mechanochemical activation of 2:1 clay minerals (such as montmorillonite, mica) for effectively improvement of their pozzolanic reactivity.

This study systematically investigates the effects of mechanochemical activation on the pozzolanic reactivity and physicochemical properties of natural kaolinite, muscovite and montmorillonite clays for developing a fundamental understanding of the process down to the atomic level. The effects of mechanochemical activation on the particle size distribution, surface texture properties, morphologies, crystal structures and atomic-level chemical structures of three typical clay minerals were investigated, combining X-ray diffraction (XRD), X-ray photoelectron spectroscopy (XPS), nitrogen adsorption porosimetry, and scanning electron microscopy with energy dispersive X-ray analysis (SEM-EDX). The physical and chemical properties, as well as performances as SCMs, of the mechanochemically activated clays were compared with both thermally activated and as-received clays, where the phase assemblages, pore structures, and mechanical performances of the blended cement pastes and mortars were also assessed.

2. Materials and experimental methods

2.1. Materials

The natural kaolinite, montmorillonite, and muscovite clays used in this study were collected from Balikesir, Eskisehir and Aydin, in Turkey. Impurities such as quartz and cristobalite are presented in these natural clays, around 20 ± 4 % for kaolinite and montmorillonite, and around 5 ± 2 % for muscovite. CEM I 42.5 R type Ordinary Portland cement from Dragon Alpha Cement (containing 5.1 % of $CaCO_3$ as quantified by thermal analysis) was used for preparing the blended cement pastes and mortars. The chemical composition of the raw materials was determined via X-ray fluorescence analysis using the fused beads method (Table 1). The loss on ignition (LOI) was evaluated by heating for 2 h at 1050 °C.

2.2. Sample preparation

2.2.1. Mechanochemical activation

The raw kaolin (KA), muscovite (MU) and montmorillonite (TN) were received in powder form from the supplier. Mechanochemical treatment of each clay mineral was performed using a Retsch PM 100 planetary ball mill with a 250 mL zirconium jar. For each activation cycle, 15 g of pure powdered clay was added to the zirconium jar and ground using 50 zirconium balls (10 mm in diameter), equivalent to a zirconium ball to clay mass ratio of 10/1. The milling speed was stabilized at 500 rpm. All three clay minerals underwent four different activation grinding times: 20, 40, 60 and 120 min. After their mechanochemical activation, the milled powder samples were immediately transferred into sealed bags and kept at room temperature (20 ± 2 °C). The mechanical friction between the milling balls during the mechanochemical activation processes can generate heat that might increase the temperature within the milling jar. To verify the extent of such effect, the surface temperature of the milling jar under the maximal mechanochemical activation condition was measured using the FLIR thermal camera (Supporting information Fig. S-2). It shows that the

Table 1
Chemical compositions of kaolinite, montmorillonite and muscovite clays determined via X-ray fluorescence analysis. LOI is Loss on Ignition at 1050 °C.

Compositions (wt%)	CEM I 42.5 R	Kaolinite (KA)	Muscovite (MU)	Montmorillonite (TN)
SiO_2	20.1	46.8	44.8	66.2
Al_2O_3	5.4	36.4	24.7	12.4
Fe_2O_3	3.0	0.4	3.1	0.8
CaO	62.8	0.3	0.4	1.4
MgO	2.2	0.1	12.9	2.4
SO_3	2.2	0.1	0.1	–
TiO_2	0.2	0.7	0.8	0.2
K_2O	0.9	0.9	3.8	0.7
Na_2O	0.1	0.1	0.9	0.6
LOI	3.4	14.2	7.8	15.3
Na_2O_{eq}	0.7	0.7	3.4	1.1

Note: $Na_2O_{eq} = Na_2O + 0.658 K_2O$.

temperature within the milling jar was between 60 °C (approximately) to the maximal 88.4 °C, with the milling ball surfaces mostly at around the maximal temperature and the inside wall of the jar at around 60 °C. This suggests the clay minerals processed during the mechanochemical activation processes might be subjected to a heating effect between this temperature range. Alongside the mechanochemical activation process, thermal activation of the raw materials was carried out for benchmarking purposes.

2.2.2. Thermal activation

For the thermal activation treatment, kaolin and montmorillonite were thermally treated at 700 and 830 °C for 3 h, respectively, while muscovite was thermally activated under 900 °C for 3 h. The 3 h calcination duration was chosen to achieve the mass loss stabilisation [37]. The samples (m = 50 g) were thermally treated at a constant heat-up rate (10 °C/min) from ambient to the aimed temperature, where the samples remained for 3 h. After thermal activation, the crucibles were removed from the oven and the activated materials were spread on a steel plate at room temperature to naturally cool down. The thermal activation temperature was determined based on the thermogravimetry analysis of the raw samples (results can be found in Fig. 5), where the temperature between the end of dehydroxylation and the beginning of recrystallisation was chosen. The thermal activation temperature used in this study is similar to that reported in literature for the same type of clays [15,38].

The activated materials were labelled as KA-(20/40/60/120/T), MU-(20/40/60/120/T) and TN-(20/40/60/120/T), where the first two letters refer to mineral, numbers correspond to the mechanochemically activation time, and T refers to thermal activation (Table 2).

2.2.3. Preparation of pastes and mortars

Blended cement pastes and mortars were prepared using mechanochemically and thermally treated clays. The mix designs used are shown in Table 3. The strength activity index was performed according to ASTM C311 [39] and a constant w/b ratio of 0.5 (by mass) was used for preparing both paste and mortar samples. Reference samples were prepared with either 100 % Ordinary Portland cement or at 20 % replacement with as-received natural clay. Mechanically milled quartz (EN 196-1 standard sand, PSD in the Supporting information Fig. S-3) was used to replace 20 % of CEM I as the inert fillers for indicating the filler effects (M-Q). The pastes were prepared using a high shear overhead mixer. The paste samples were cured in sealed plastic containers at room temperature (20 ± 2 °C) for 28 days. The mortar samples were produced using BS EN 196-1 standard [39] with a binder to sand ratio of 1:3, and cast using 40 mm × 40 mm × 40 mm moulds.

Table 2
Activation characteristic of materials.

Series	Type of activation	Duration (min)	Temperature (°C)
KA-20	Mechanochemical activation	20	Ambient
KA-40		40	Ambient
KA-60		60	Ambient
KA-120		120	Ambient
KA-T	Thermal activation	180	700 °C
MU-20	Mechanochemical activation	20	Ambient
MU-40		40	Ambient
MU-60		60	Ambient
MU-120		120	Ambient
MU-T	Thermal activation	180	900 °C
TN-20	Mechanochemical activation	20	Ambient
TN-40		40	Ambient
TN-60		60	Ambient
TN-120		120	Ambient
TN-T	Thermal activation	180	830 °C

Table 3
Mix designs for pastes and mortars (for every 100 g of solid binders).

Sample ID[a]	CEM I (g)	SCMs (g)	Type of materials as SCMs	Water (g)	Sand (g)
P-PC	100	0	None	50	0
M-PC	100	0	None	50	300
M-Q	80	20	Quartz (milled EN 196-1 standard sand) as inert fillers (D_{50} = 10.4 μm)	50	300
P-KA-R	80	20	Kaolin as received	50	0
M-KA-R	80	20		50	300
P-KA-60	80	20	Kaolin after 60 min mechanochemical activation	50	0
M-KA-60	80	20		50	300
P-KA-T	80	20	Kaolin after thermal activation at 700 °C	50	0
M-KA-T	80	20		50	300
P-MU-R	80	20	Muscovite as received	50	0
M-MU-R	80	20		50	300
P-MU-60	80	20	Muscovite after 60 min mechanochemical activation	50	0
M-MU-60	80	20		50	300
P-MU-T	80	20	Muscovite after thermal activation at 900 °C	50	0
M-MU-T	80	20		50	300
P-TN-0	80	20	Montmorillonite as received	50	0
M-TN-0	80	20		50	300
P-TN-60	80	20	Montmorillonite after 60 min mechanochemical activation	50	0
M-TN-60	80	20		50	300
P-TN-T	80	20	Montmorillonite after thermal activation at 700 °C	50	0
M-TN-T	80	20		50	300

[a] In the sample ID, "P" refers to paste samples while "M" refers to mortar samples.

2.3. Test methods

Particle properties such as size and surface texture of the three different types of clays before and after the activation processes (mechanochemically and thermally) were characterised using the particle size distribution, scanning electron microscope (SEM) imaging and N_2 adsorption. Thermogravimetry analysis (TG), XRD, Fourier-transform infrared spectroscopy (FTIR) and XPS were used to monitor the changes in the chemical structure of all three clay minerals upon the effect of the different activation methods. The 28-day blended cement pastes were characterised using XRD, TG, and FTIR. Before characterisation, the paste samples were crushed and immersed in isopropanol for 15 min and stored under vacuum for 24 h. The pore size distribution of the blended cement mortar was assessed using the mercury intrusion porosimetry (MIP). The compressive strength of the mortar cubes was evaluated at 28 days of curing using a Utest 6410 instrument according to EN 196-1. The pozzolanic reactivity of the activated clays was determined using the bound water method specified in the ASTM C1897 – 20 (also known as the R^3 test) [40]. Specifications of each of these test methods can be found below.

2.3.1. Particle size distribution and surface properties

The particle size distribution (PSD) of powdered clay minerals before and after activation was determined with a Malvern Mastersizer 2000. Both mechanochemically and thermally treated kaolin, montmorillonite and muscovite minerals were dispersed in distilled water for characterisation. Five minutes of ultrasonication was carried out for all minerals before particle size measurement.

The surface textural properties of mechanochemical and thermal activated clay minerals were characterised using the N_2 gas sorption at 77 K using the Autosorb-iQ-C from Quantachrome Anton Paar. The specific surface area of the characterised samples was determined using the Brunauer-Emmett-Teller (BET) method. Prior to the gas sorption test, the mechanochemically and thermally activated clay minerals were degassed under vacuum at 30 °C for 16 h.

The surface morphology of the activated clay minerals was

characterised using SEM. First, the powdered samples were mounted on conductive carbon tape and then coated with 99 % pure gold (Au) for 150 s in an argon gas environment using a coating device (Quorum, SC-7620). The surface morphology of the coated samples was examined using the JEOL JSM 6610 SEM under vacuum with an acceleration voltage of 15 kV.

2.3.2. Spectroscopic analysis (XRD, FTIR and XPS)

The crystal structures of the powdered samples were determined by the Rigaku-SmartLab X-ray diffractometer using Cu-Kα radiation with a wavelength of 1.5408 Å. The tests were conducted with a step size of 0.02° and a counting time of 3 s/step, from 5° to 60° (2θ).

The FTIR results were obtained using the attenuated total reflection (ATR) method with a PerkinElmer Spectrum 100 Instrument. The FTIR spectra were recorded between wavenumber 600 and 4000 cm^{-1}, with a resolution of 4 cm^{-1}. The results of 10 accumulative scans were reported for each sample tested.

XPS analysis was performed at HarwellXPS facility (UK) for surface characterisation. The samples in powder form were fixed on adhesive tape and analysed "as received" and characterised under vacuum conditions. The monochromatic Al Kα radiation (1486.6 eV) was used for photoelectron emission. The survey scans were performed at a binding energy range between −1.5 eV and 1203.5 eV, with the pass energy of 160 eV, energy step of 1.0 eV, and the dwell time of 99.5 ms. The high-resolution scans of Al2p, Si2p and O1s spectra were collected with the constant analyser pass energy of 20 eV, energy step of 0.1 eV. The dwell time for these three elements (Al2p, Si2p and O1s) was 271.5 ms, 350.9 ms, and 298.5 ms. All the spectra were recorded at take-off angles of 90°. For the characterised results, the binding energy values were charge-corrected to the C1s signal, set at 284.8 eV. Sample charging was also checked by recording C1s spectra both before and after the accumulation of each narrow scan spectrum, where the variation differences were kept under 0.1 eV.

2.3.3. Thermal analysis

The thermogravimetric measurements of the raw and activated clay minerals were conducted using the Netzsch Sta 449F1, while the blended cement samples were characterised using a SII Exstar 6000 machine. However, the identical testing program was used, where 20 mg of powdered samples were used for each test, heated from 50 °C to 950 °C at the constant heating rate of 10 °C/min in the N_2 gas at the flow rate of 30 mL/min. The equation given below was used to calculate the mass of portlandite in the blended cement pastes, where $m_{Ca(OH)_2}$ and $m_{(H_2O)}$ are the molecular weight of portlandite and water respectively, and $ML_{Ca(OH)_2}$ is the mass loss between 400 °C and 500 °C determined from the thermogravimetry measurement. The "Mass of portlandite reduced (%)" shown in Fig. 13D was determined by subtracting the remaining portlandite mass percentage in each sample from the total portlandite mass percentage in the 100 % CEM I portland cement paste (P-PC, as shown in Table 3)

$$Ca(OH)_2 = ML_{Ca(OH)_2} \frac{m_{Ca(OH)_2}}{m_{(H_2O)}} = ML_{Ca(OH)_2} \frac{74}{18}$$

2.3.4. MIP

The MIP measurements were performed using the Thermo Scientific Pascal 440 Series instrument. The 28 day blended cement mortars were crushed into small pieces (about 0.50 g in mass and 2 mm in size). The crushed mortar samples were immersed in isopropanol for 24 h, followed by vacuum drying for 24 h. The external pressure range from 0.10 MPa to 400 MPa was used, with the mercury contact angle and surface tension of 140° and 0.48 N/m, respectively. The accumulative pore volume and pore size distributions of the 28 days blended cement mortars were determined from the MIP results.

2.3.5. R^3 test and mechanical properties

The pozzolanic reactivity of the clay minerals assessed in this study was determined using the bound water test method, specified as part of the R^3 test [40,41]. For each SCM precursor, the bound water content was determined by mixing SCM with $Ca(OH)_2$, KOH, K_2SO_4, $CaCO_3$ and deionised water. Then the R^3 pastes were kept in sealed containers at 40 °C for seven days. After seven days of reaction, the crushed hydrated samples dried in an oven at 105 °C to reach constant weight. Finally, the dried samples were heated at 350 °C for 2 h, and the weight differences were used to determine bound water. Compressive strength tests were carried out for 28 days with a loading rate of 6 Ns^{-1}. Three cubes (specimens) were tested for each mortar mix designs.

3. Results and discussion
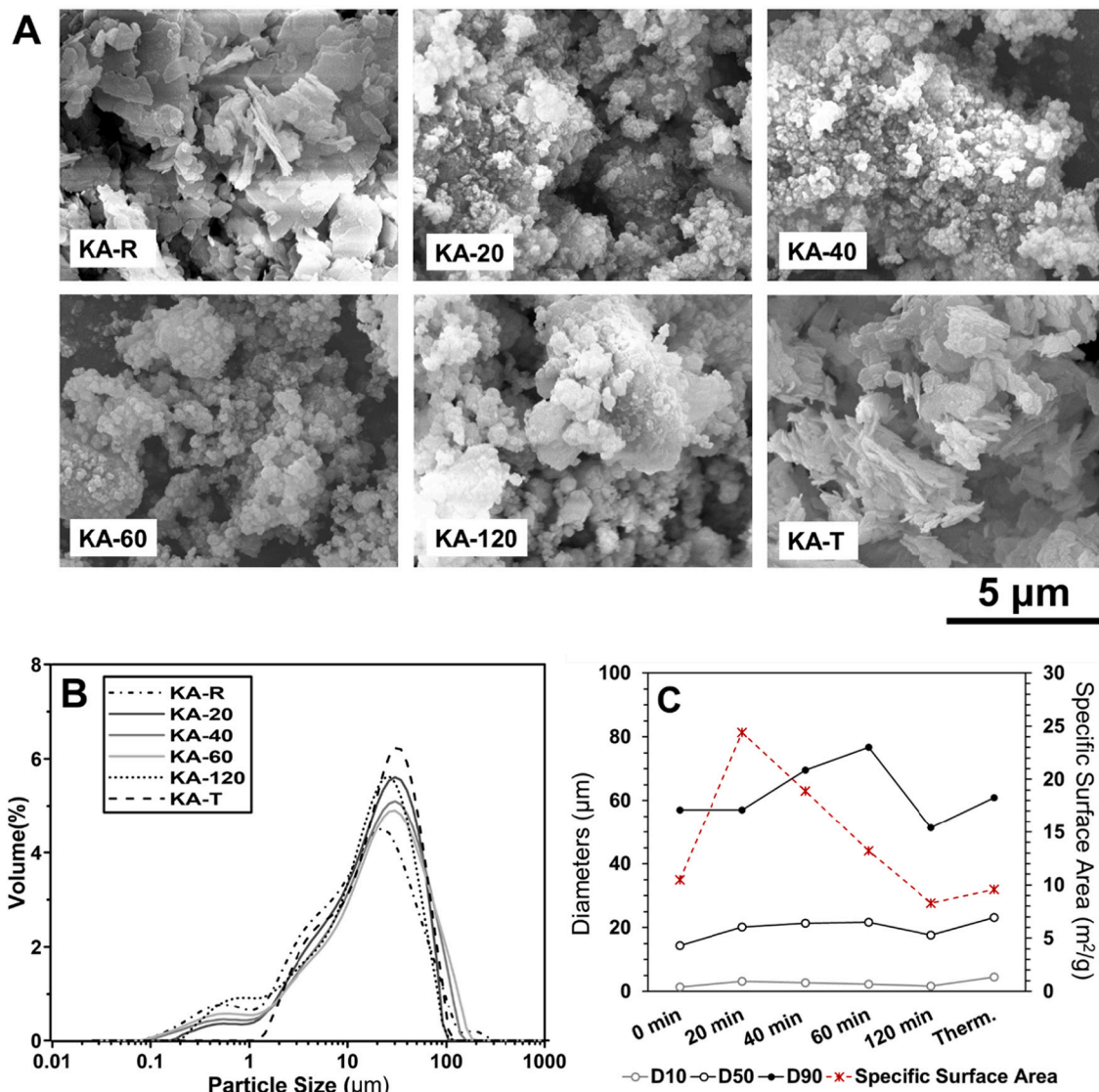
3.1. Mechanochemical activation

3.1.1. Particle size distribution and surface texture properties

Figs. 1 to 3 summarise the effects of mechanochemical activation on the surface morphology, particle size distribution (PSD), and specific surface areas of the three minerals investigated, in comparison to their thermally activated and as-received counterparts.

The natural kaolin (KA-R) showed hexagonal sheet-type morphology, which did not change significantly after the thermal treatment at 700 °C (KA-T). The thermally activated kaolin resembles more of a lamellar structure rather than a semi-spherical one, similar to that reported by Souri et al. [18], where particles with rounded edges and defected hexagonal platelets with apparent agglomeration of smaller particles on the surfaces were observed. For the mechanochemically treated kaolin, small close-to-spherical particles agglomerated into larger particles were formed after the initial 20 min of mechanochemical milling, which can be attributed to the delamination of kaolin particles [18,42]. The further increase of the mechanochemical milling time from 20 min to 120 min did not appear to significantly further modify the particle morphology, except that the size of the close-to-spherical particles agglomerated on the surface slightly increased. The overall shape of the PSD curve did not change substantially after either activation methods. In comparison with the as-received kaolin mineral (Fig. 1B), both the mechanochemical activation and the thermal activation treatment slightly increased the overall particle sizes. As shown in Fig. 1C, as the milling time increased from 20 min to 60 min, the median diameter (D_{50}) values increased from 14.3 μm (as-received) to 21.7 μm. After 120 min of milling, the D_{50} value decreased to 17.6 μm. Similar trends can be found from the D_{10} and D_{90} values, showing consistent change across the full range of particle sizes. During this process, the specific surface area of kaolin increased from 10.5 m^2/g to 24.4 m^2/g after the initial 20 min of milling. Beyond 20 min, the specific surface areas gradually decreased to 8.3 m^2/g as the time of milling increased. As for the thermally treated kaolin, only a marginal difference was observed (9.6 m^2/g).

The slight decrease of specific surface area after thermal treatment can be attributed to the sintering and agglomeration that arises during the heating and cooling process [18]. The substantial increase of specific surface area after 20 min of mechanochemical activation can be attributed to the decrease in particle size by the mechanical effect that delaminates the kaolinite layered structures [43,44]. As the milling time increases, the formation of the round-edge particles with rugged surfaces resulted in larger-sized agglomerated particles on the surface [43,44], leading to a reduction in specific surface areas while the overall PSD stayed relatively unchanged. Similar phenomena were also reported by Souri et al. [18] using kaolin sourced from Zonouz (northwest of Iran) and Zettlitz (Czech Republic). However, depending on the particle sizes of the starting materials and the configuration of the high impact ball mill used, shorter or longer milling time might be required to reach the maximal specific surface areas before the agglomeration phenomena start to occur [45–47]. The increased formation of
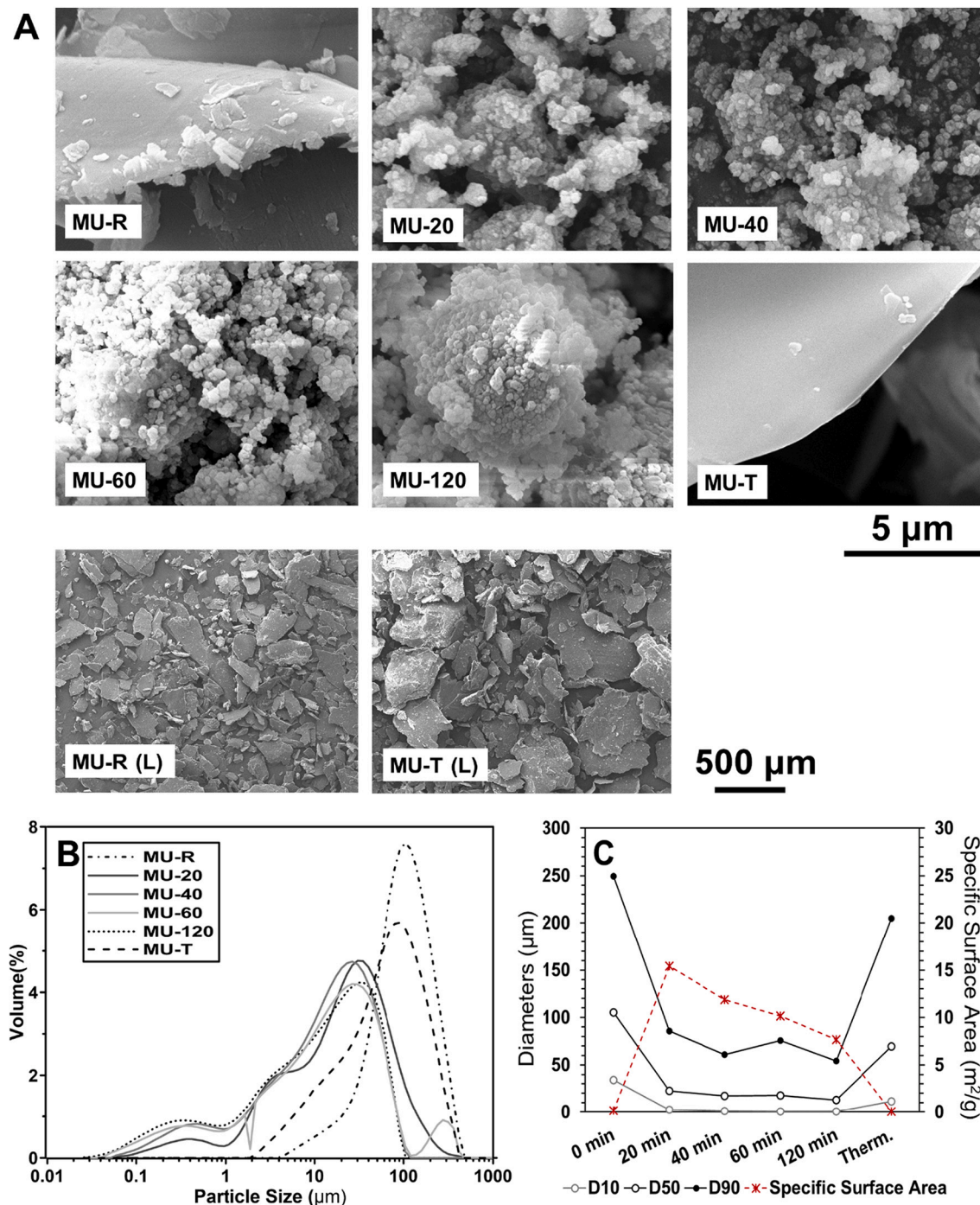
Fig. 1. Kaolin SEM images (A), particle size distributions (B), and characteristic diameters (C) D10, D50, D90 and the BET specific surface area of as-received (0 min), mechanochemically (20, 40, 60 and 120 min) and thermally activated (therm) kaolin. The original data for production of (C) can be found in the Supporting Information document.

amorphised agglomerates might be responsible for the decreases in measured specific surface areas, as the high energy milling process can result in bonds between agglomerates that are difficult to be separated by chemical dispersant or ultrasound [33].

Fig. 2 summarises the result for muscovite minerals. The natural muscovite used in this study showed irregular sheet-type morphology with the D_{50} values around 105.2 μm. The plate-like shape of the muscovite might affect the representativeness of the particle sizes values presented, but the relative changes between different samples are the key factor under consideration here. The thermal treatment at 900 °C for 3 h did not seem to alter their as-received morphology significantly, similar to that observed for kaolin minerals. However, the sheet-type morphology was completely destroyed after 20 min of mechanochemical activation, with the D_{50} value immediately decreased to 22.8 μm. Despite the similarity in surface morphology changes, the evolutions of PSD under the various activation conditions are very different to that of the kaolin minerals. The particle size reduction after thermal treatment observed from the muscovite sample is likely due to its relatively larger original particle size (in comparison with the other two materials), where the contraction effect due to heating and cooling likely surpassed the aggregation effect [48]. While the thermal activation process slightly

decreased the overall particle sizes, the mechanochemical activation substantially decreased the PSD within the initial 20 min of activation and changed the overall shape of the PSD curves. On the other hand, increasing the mechanochemical activation time to 120 min did not seem to have significant impact on the PSD. Agglomerated particles within two size ranges were formed in mechanochemically treated muscovite, a small fraction between 0.1 and 1.0 μm, and the majority between 1 and 100 μm. The formation of small agglomerated particles within the 0.1 to 1.0 μm range is particularly significant for the muscovite minerals investigated in this study, as the smallest particle size characterised in the as-received muscovite was around 4 μm. As shown in Fig. 2C, the specific surface area of muscovite increased from 0.2 m²/g to 15.4 m²/g after the initial 20 min of milling. At 120 min milling time, the specific surface areas decreased to 7.6 m²/g, same as that observed from the kaolin. Similar phenomena were also observed for mechanically activated muscovite samples [34]. The results here suggest that for muscovite, the change of specific surface area during mechanochemical activation is not exclusively due to the change in PSD, but also relates to changes in the surface texture properties. Similar behaviour has also been reported by Andric et al. [44], where modifications of both particle size and surface texture properties were
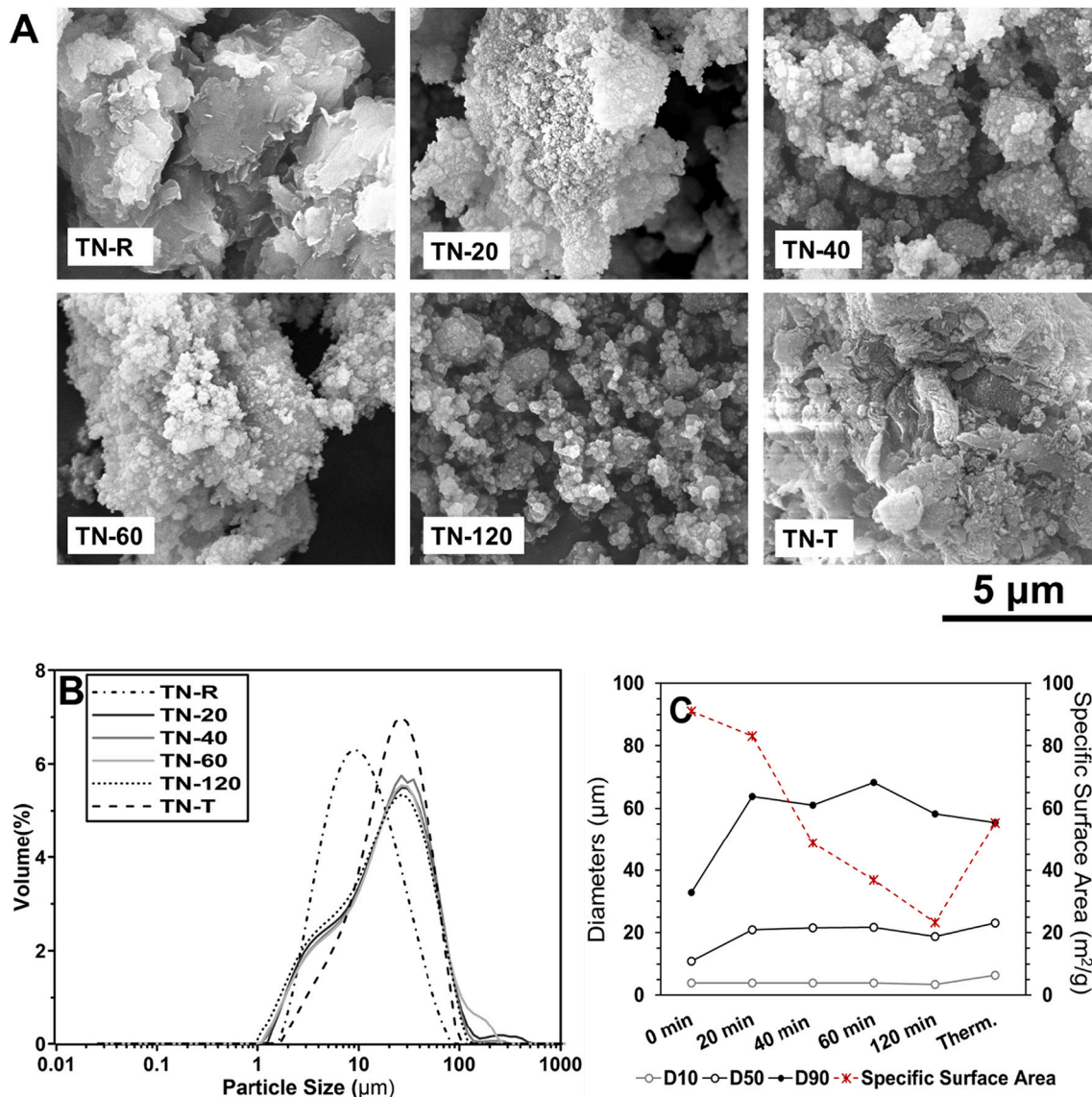
Fig. 2. (A) Muscovite SEM images, (B) particle size distributions, and (C) characteristic diameters D10, D50, D90 and the BET specific surface area of as-received, mechanochemically and thermally activated muscovite. MU-R(L) and MU-T(L) are the SEM images of as-received and thermally activated muscovite at lower magnification respectively. The original data for production of (C) can be found in the supporting information document.

observed.

Fig. 3 summarises the result for montmorillonite minerals. The natural montmorillonite minerals demonstrated irregular and sheet-type morphology, similar to that reported in the literature [49]. Thermal activation treatment led to significant coarsening of surface morphology while some level of the sheet-type morphology remained. The mechanochemical activation treatment used in this study effectively delaminated the montmorillonite particles within the initial 20 min of milling, resulting in the formation of very fine close-to-spherical particles agglomerated on the surfaces. As the milling time increased, the size of these spherical particles increased due to agglomeration under

mechanical impact; nevertheless the overall size of these agglomerated particles was much smaller than that observed from kaolin and muscovite under the same milling time. The PSD results shown in Fig. 3B suggest that both thermal and mechanochemical activation have increased the overall size distribution of the particles. The as-received montmorillonite showed near normal distribution on a log scale with a D_{50} value of 10.9 μm. After the thermal treatment, the D_{50} value increased to 23.0 μm. After the thermal activation, the overall shape of the PSD remained largely unchanged. Whereas for the mechanochemical activation, the PSD changed from near to normal distribution to bimodal distribution on the log scale. This behaviour is similar to that

Fig. 3. The (A) SEM images, (B) particle size distributions, and (C) characteristic diameters D10, D50, D90 and the BET specific surface area of as-received, mechanochemically and thermally activated montmorillonite. The original data for production of (C) can be found in the Supporting Information document.

observed from the muscovite, however, small particles within the 0.1 to 1.0 μm range were not observed for the activated montmorillonite samples. Dellisanti et al. [49] also observed the increase of overall particle size distribution after mechanochemical treatment of Ca-montmorillonite, without identifying the bimodal distribution. Instead, their study identified a small fraction of particles within the 0.5 to 1.0 μm range after milling for 20 h. The absence of small particles within this range in the mechanochemically treated montmorillonite used for this study might be due to the much shorter milling time.

The specific surface areas shown in Fig. 3C correlate well with the overall particle size distributions, where larger particles generally result in lower specific surface area. For mechanochemically treated samples, the surface morphology has more significant impact on the specific surface area, which decreased as the milling time increased. This trend is consistent with that observed from kaolin and muscovite samples. However, while having similar D_{50} values to kaolin under respective treatment conditions, the montmorillonite samples showed much higher specific surface areas, with a maximum 91.0 m^2/g for the as-received and the minimum 23.3 m^2/g for the 120 min mechanochemically activated montmorillonite. The much finer spherical particles (below 0.1 μm according to the scale bar) on the surfaces in comparison with kaolin

and muscovite might also increase the overall specific surface areas after mechanochemical activation.

It is worth noting that, despite the as-received minerals have different particle sizes, the D_{10}, D_{50} and D_{90} values after mechanochemical activation were within a similar size range and not affected substantially by the increase of the milling time, e.g. around 20 μm D_{50} for the three different minerals. The structural, surface, and chemical properties of the milled materials is consistent with the studies conducted by Suraj et al. [46], Vdovic et al. [50] and Sondi et al. [51], where the clay minerals with different original structures, surface and chemical properties showed similar morphological and surface characteristics after prolonged milling time. These authors also reported the formation of amorphous aluminosilicate with similar structural, morphological and surface characteristics after extended grinding. Besides, some SEM images suffered from local charging effect which might shadow the morphology of the fine particles on the sample surfaces in some locations. Further investigations using the transmission electron microscopy might help further illustrate the morphology of the fine particles on surface of the mechanochemically treated samples.

3.1.2. Evolution of chemical structures

The mineralogy and gel structure of as-received, mechanochemically and thermally treated kaolin, muscovite and montmorillonite minerals were characterised using the XRD, as shown in Fig. 4. The XRD pattern of as-received kaolin (Fig. 4A) indicates the presence of mainly kaolinite (Powder diffraction file, PDF# 79-1570) and a small amount of illite (PDF# 26-0911) and quartz (PDF# 79-1910 and 79-1911). The results show that the mechanochemical process was able to effectively delaminate and amorphised the crystal structure of the as-received kaolin during the initial 20 minutes of activation, as indicated by the significant reduction of the d[001] and d[002] reflection peaks. The multiple reflection peaks between 19° and 22° (2θ) were amorphised into one broad hump centred at 20°, which was further amorphised and reduced as the mechanochemical activation time increased from 20 to 120 min. Similar crystal structure evolution was also observed in literature for kaolinite minerals sourced from other locations [18]. The trace illite phase completely disappeared after 20 min of mechanochemical activation but the quartz phase remained unaffected even after 120 min of mechanochemical activation. In comparison with the thermally treated kaolin, the thermal process (700 °C for 3 h) was able to destroy the crystal structure and dehydroxylate the kaolin but not the illite phase. This is because the thermal destruction of illite requires much higher temperature (at least 930 °C) [7]. Quartz peaks are also preserved, which suggests that quartz was not affected by the thermal process. These results are consistent with the literature reported for thermally activated kaolinite [36].

As shown in Fig. 4B, the natural muscovite mineral used in this study also contains significant amount of vermiculite (PDF# 16-0613) in addition to muscovite (PDF# 82-0576), both of which belong to the mica mineral group and exhibit similar morphology. A small fraction of the quartz phase was also observed, which did not alter after the mechanochemical activation treatment. In contrast, the reflection peaks representing vermiculite and muscovite broadened and reduced significantly after 20 min of mechanochemical activation, disappearing completely after 60 min of treatment. These changes in the crystallinity of the structure are likely to be attributed to the delamination, dehydroxylation and amorphisation of the layered mica structures, similar to that observed from prolonged grinding of muscovite [34]. As for the thermally treated natural muscovite (900 °C for 3 h), the vermiculite peaks disappeared after calcination in consistency with that reported in the literature [52]. However, it is essential to note that the thermal activation temperature used in this study for muscovite was unable to destroy its crystal structure even after dehydroxylation, similar to that observed by Fernandez et al. [7]. The presence of large flaky shaped clay particles, as depicted in Fig. 2, corresponds to the identification of muscovite with unchanged laminated crystalline structure after thermal activation from the XRD.

The as-received natural montmorillonite (Fig. 4C) also contains quartz and cristobalite (SiO$_2$ polymorph, PDF# 39-1425). After the initial 20 min of mechanochemical activation, the intensity of the reflection peaks representing montmorillonite, especially the basal reflection peak at d[001], decreased and turned into a broad, amorphous hump. This suggests a change from a crystalline into an amorphous structure. Beyond the 20 min of mechanochemical activation, the montmorillonite peaks disappeared entirely. However, the reflection peaks for cristobalite and quartz phases showed negligible broadening and decreasing in intensities. The thermal activation treatment resulted in the reduction of the basal space, shifted from 13.2 Å (6.7°) to 9.7 Å (9.1°), but the laminated crystal structure remained. The thermally treated montmorillonite showed a similar crystal structure to that of illite, identical to that reported in the literature at the calcination temperatures between 650 °C and 830 °C [7,53].

The thermogravimetric analysis (TGA) results are shown in Fig. 5. The as-received kaolin, muscovite, and montmorillonite showed major dehydroxylation mass loss peaks centred at 520 °C, 880 °C and 690 °C, respectively. These findings are consistent with that observed in the
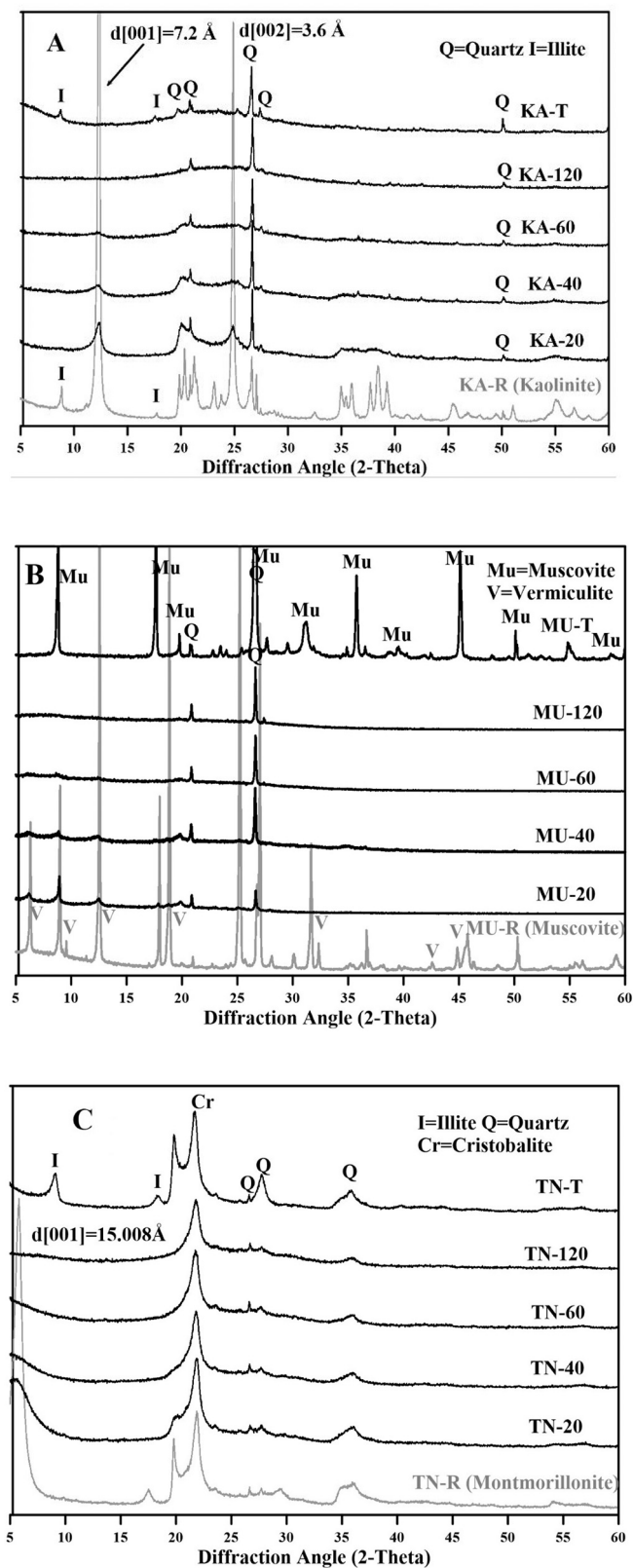

Fig. 4. XRD analysis of original, mechanochemical activated and thermally activated A) kaolin, B) muscovite and C) montmorillonite, where I: illite, Q: quartz, Mu: muscovite, V: vermiculite and Cr: cristobalite.
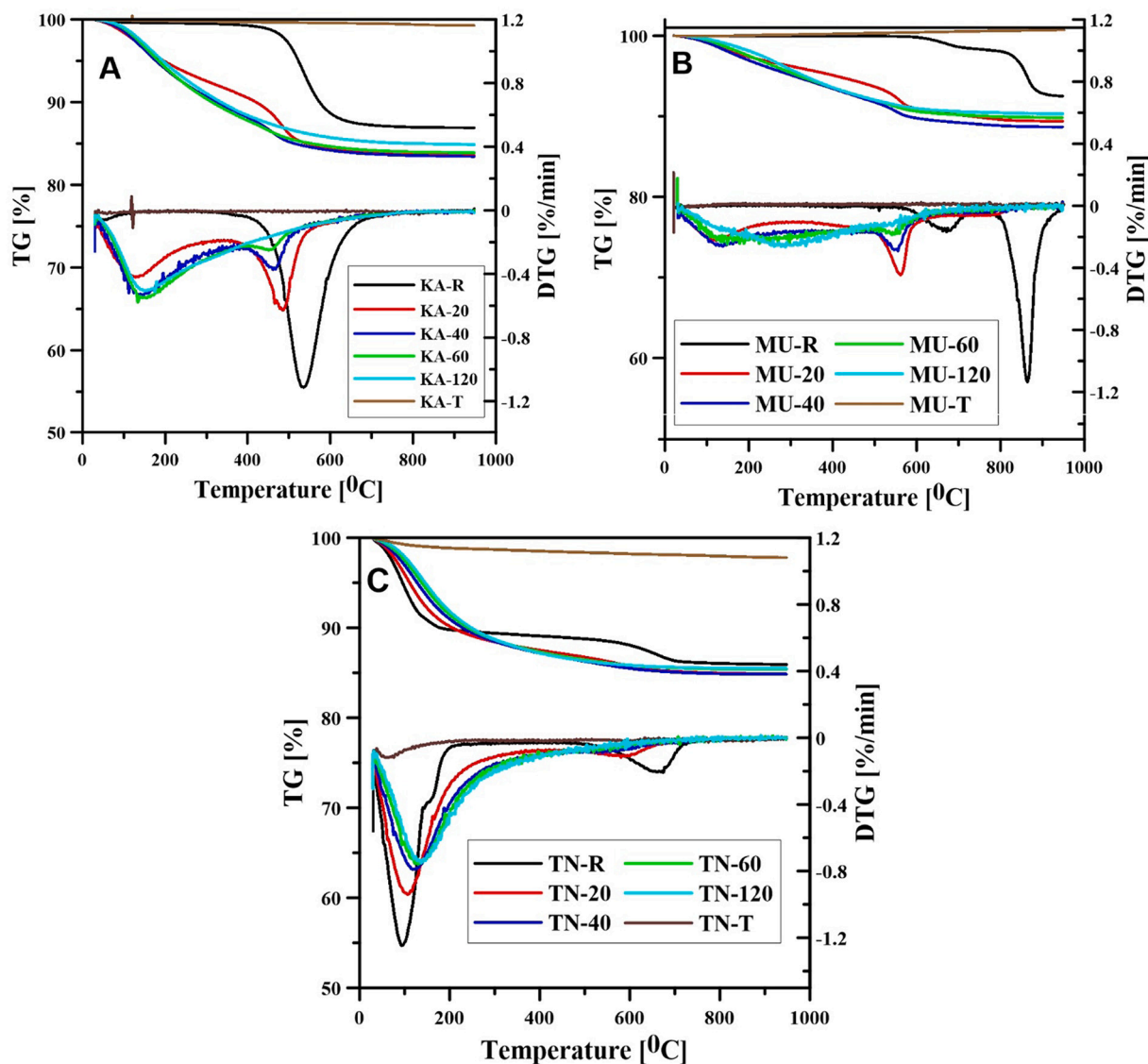
Fig. 5. TGA analysis for as-received, mechanochemical and thermally treated A) kaolin, B) muscovite, and C) montmorillonite showing TG (top) and DTG (bottom) for each material.

literature [18]. For the as received montmorillonite, the mass loss at 150 °C is attributed to the loss of physically absorbed water molecules. The appearance of two dehydration peaks is caused by the presence of mixed multivalent cations in the interlayers [54–56]. The thermally treated samples showed a negligible mass loss from the TGA, suggesting effective thermal treatment under respective thermal treatment temperature for each of the minerals assessed. The increase of mechanochemical treatment from 20 min to 120 min showed a similar impact on the dehydroxylation peaks among all three minerals. As the milling time increased, the dehydroxylation peaks shifted towards lower temperatures and decreased in intensity. This suggests that mechanochemical treatments reduce the energy required for decomposing the hydroxyl groups and remove part of the hydroxyl groups during the high impact milling process. This corroborates with the XRD results where delamination and amorphisation were observed. Therefore, structural disorder and the delamination of the minerals reduce the dehydroxylation temperature by weakening the OH bonds [57]. In turn, a decrease of mass loss due to dehydroxylation, and increase of mass loss due to loss of physically absorbed water (below 200 °C) has been noted. This phenomenon can be attributed to the fact that the mechanochemical treatments were performed in closed grinding jars. The decomposed

hydroxyl groups combined to form H_2O, which was absorbed back onto the surface of the mechanochemical treated minerals. In addition, the mechanochemical treatments also seem to improve the minerals' capacity to absorb moisture from the atmosphere, as the total mass loss of the mechanochemically treated samples were higher than that of the as-received samples. This can be attributed to the increase of freshly created surfaces during the milling process, which increased the overall water absorption capacity under relative humidity [9,18]. Similar phenomena were observed in the literature for mechanochemically treated minerals [19,31,58].

The evolution of chemical structures of the bulk mineral samples before and after different activation treatments were characterised using the FTIR spectra (Fig. 6). The bands between 3600 and 3700 cm^{-1} are attributed to the stretching vibration of the interlayer hydroxyl groups [59,60]. The bands between 3400 and 3430 cm^{-1} and 1620 to 1640 cm^{-1} are assigned to the stretching and bending vibrations of O—H bonds in water. The bands between wavenumber 1200–600 cm^{-1} correspond to the stretching and bending vibrations of T(Si, Al)—O bonds [60]. For kaolin, the vibration bands at 3620, 3650 and 3695 cm^{-1} are assigned to the stretching vibration of interlayer hydroxyl groups (Al—OH bonds), while the band at 915 cm^{-1} is attributed to the
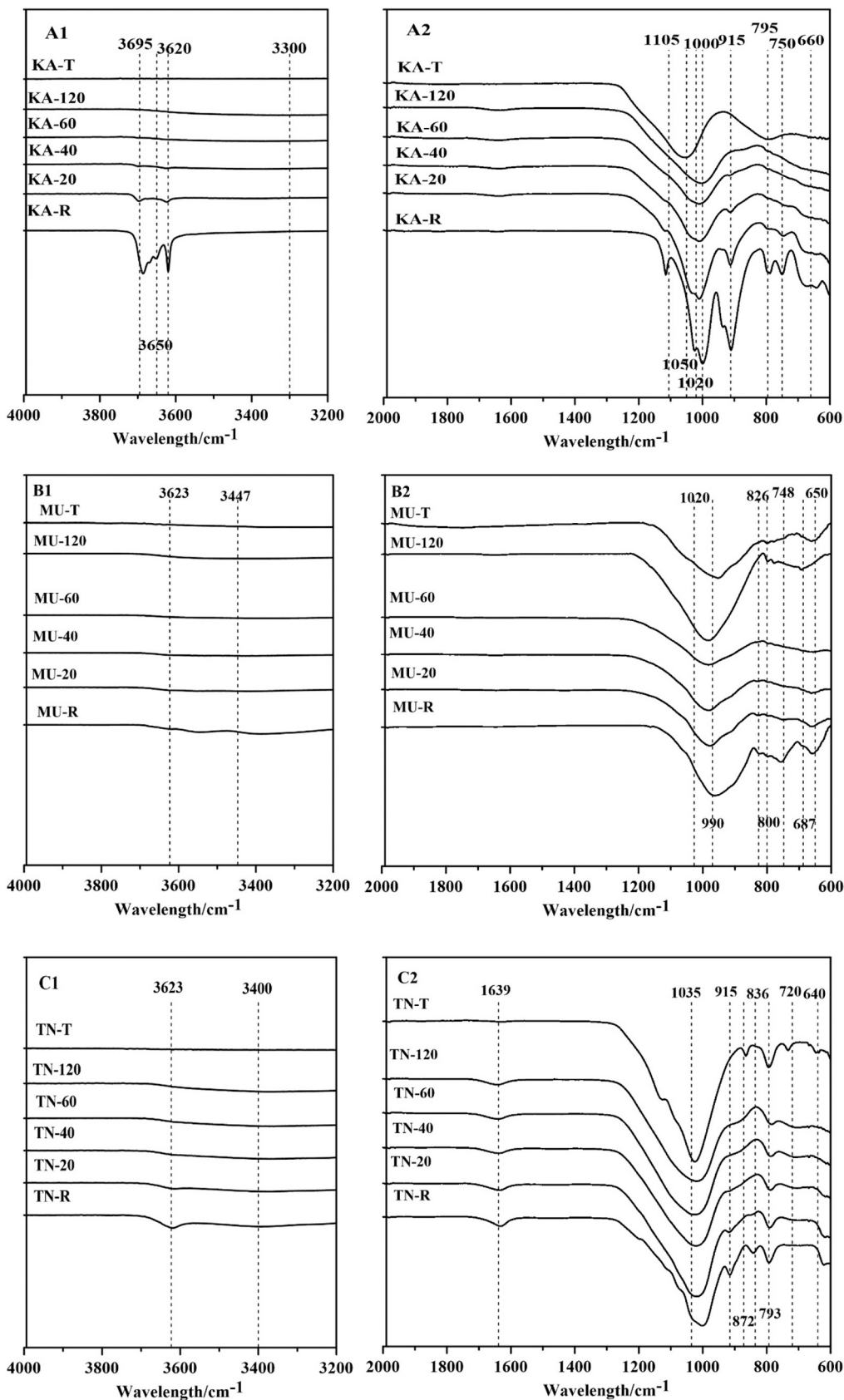
Fig. 6. FTIR spectra of the as-received, mechanochemical and thermally activated A) kaolin, B) muscovite, and C) montmorillonite showing 3200–4000 (left) and 600–2000 (right) wavelength regions of each material.

bending vibration of the same bands [19,31,61]. Significant reduction in these bands after either thermal or mechanochemical treatment suggests the removal of interlayer hydroxyls, which normally leads to the collapse of the layered mineral structures [31]. For mechanochemically treated samples, the formation of (weak) new O—H stretching bands at 3440 and 1639 cm^{-1} are attributed to the stretching and bending vibration of surface adsorbed water molecules on the surfaces, consistent with that observed from TGA results (Fig. 5). The Si—O stretching vibration bands at 1000, 1020 and 1105 cm^{-1} broadened with increased mechanochemical activation. This broadening phenomenon can be attributed to the distortion and destruction of kaolinite structure [18,62]. Also, the bands at 660, 750 and 790 cm^{-1} are attributed to the Si-O-Si stretching and bending vibration bands in the kaolin lattice layers, the disappearance of which corresponds to the structural collapse of kaolinite and the formation of amorphous hydrous aluminosilicate compounds [57]. The mechanochemically activated kaolin only showed a broad band for the Si—O—T(Si/Al) bonds centred at 1000 cm^{-1}. In comparison, the thermally treated kaolin showed a broad band centred at 1050 cm^{-1}, suggesting Si—O—T(Si/Al) bonds with higher degree of polymerisation [63].

As for the as-received muscovite (MU-R) (Fig. 6 B1and B2), the bands at 3623 and 915 cm^{-1} are assigned to the interlayer Al—OH bonds; bands at 1026, 990 and 800 cm^{-1} are assigned to the O—Si bands in the tetrahedral layers, while 826 and 748 cm^{-1} are attributed by the Al—O and Al—O—Al bands (Al in tetrahedral sheet) [34,60]. Similar to that observed in kaolin, the hydroxyl vibration bands at above 3600 cm^{-1} started to decrease as the mechanochemical milling time increased, due to partial dehydroxylation [55]. The bands at 990, 826, 800, and 748 cm^{-1} decreased and broadened with milling time, which can be attributed to the structural disorder of muscovite [9,31]. The grinding of muscovite led to the rearrangement and activation of the Al—OH bond, as well as the migration of hydroxyl from the inner part of the mineral to the mineral surface while forming molecularly-bound water [64]. In comparison with the thermally treated muscovite, the main differences occurred in the range between 600 cm^{-1} to 830 cm^{-1}, where the disappearance of bands at 748 and 650 cm^{-1} might relate to the breaking of Al—O—Al bands during mechanochemical activation. However, the thermal process did not significantly affect these bonds [7].

The bands at 3623 and 915 cm^{-1} observed from the as-received montmorillonite are attributed to the stretching and bending vibration of interlayers Al—OH bonds. The band at 836 cm^{-1} is likely attributed to the bending vibration of Mg-OH bonds due to the presence of Mg^{2+} as interlayer cations (Table 1) [59]. The reduction of these bands after either mechanochemical or thermal activation indicates the dehydroxylation of interlayer hydroxyl species, resulting in destruction of the octahedral sheet layer and releasing of the octahedrally coordinated Al [61]. The broadening of the bands attributed by the T(Si/Al)—O—Si are more prominent for mechanochemical activated samples. Additionally, these samples also show the presence of physically adsorbed water as indicated by the band at 1639 cm^{-1} (O—H in water molecules). The centres of the T(Si/Al)—O—Si bands in the region between 900 and 1200 cm^{-1} shifted to higher wavenumbers after activation treatments, with negligible difference between the two activation methods assessed.

XPS was used to investigate the effects of the different activation methods on changing the chemical structure of all clay samples at the surface level (around 5–10 nm deep). The high resolution Al2p and Si2p XPS spectra of these three types of mineral under different treatment conditions are summarised in Figs. 7 and 8. As shown in Fig. 7, the evolution of binding energy of Al2p in kaolin samples performed differently comparing to that of muscovite and montmorillonite under respective treatment conditions. For kaolin, the as-received sample presented a symmetric peak centred at 74.5 eV, similar to that reported in the literature [65]. The mechanochemical activation treatment led to broadened Al2p peak while the peak centre remained relatively unchanged. Increasing the milling time from 20 to 60 min did not seem to
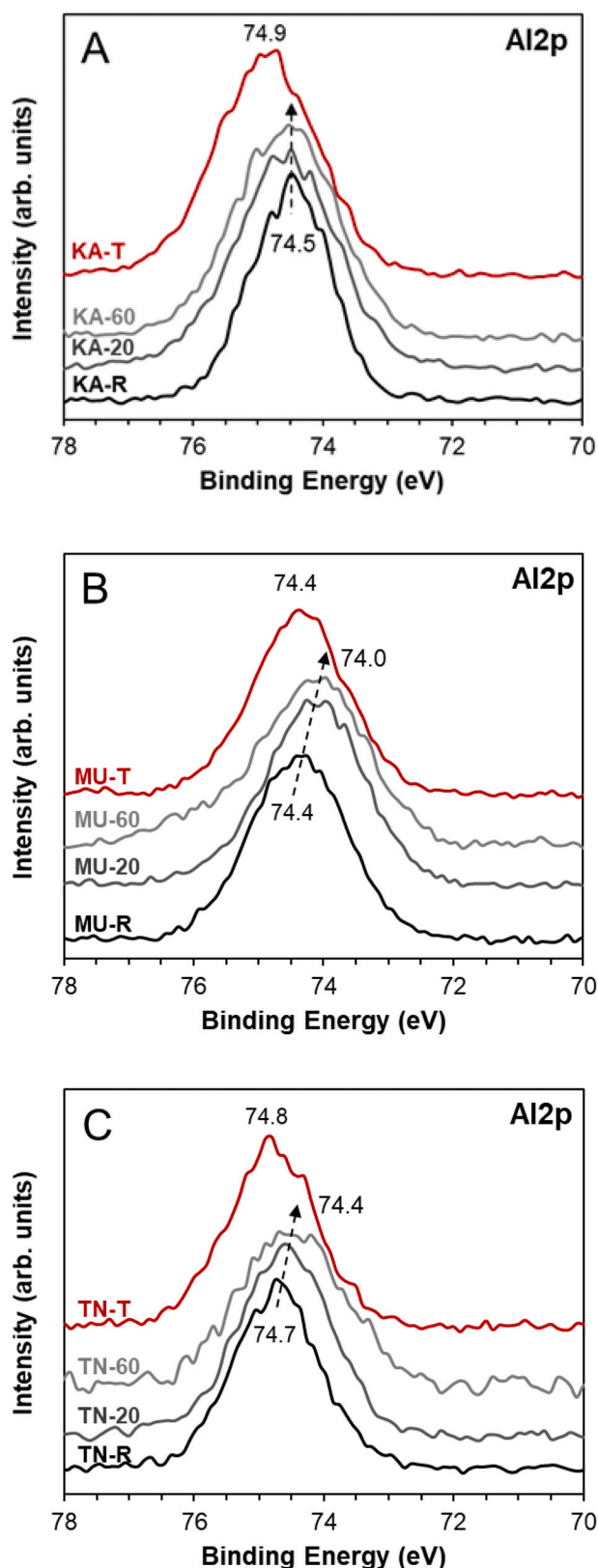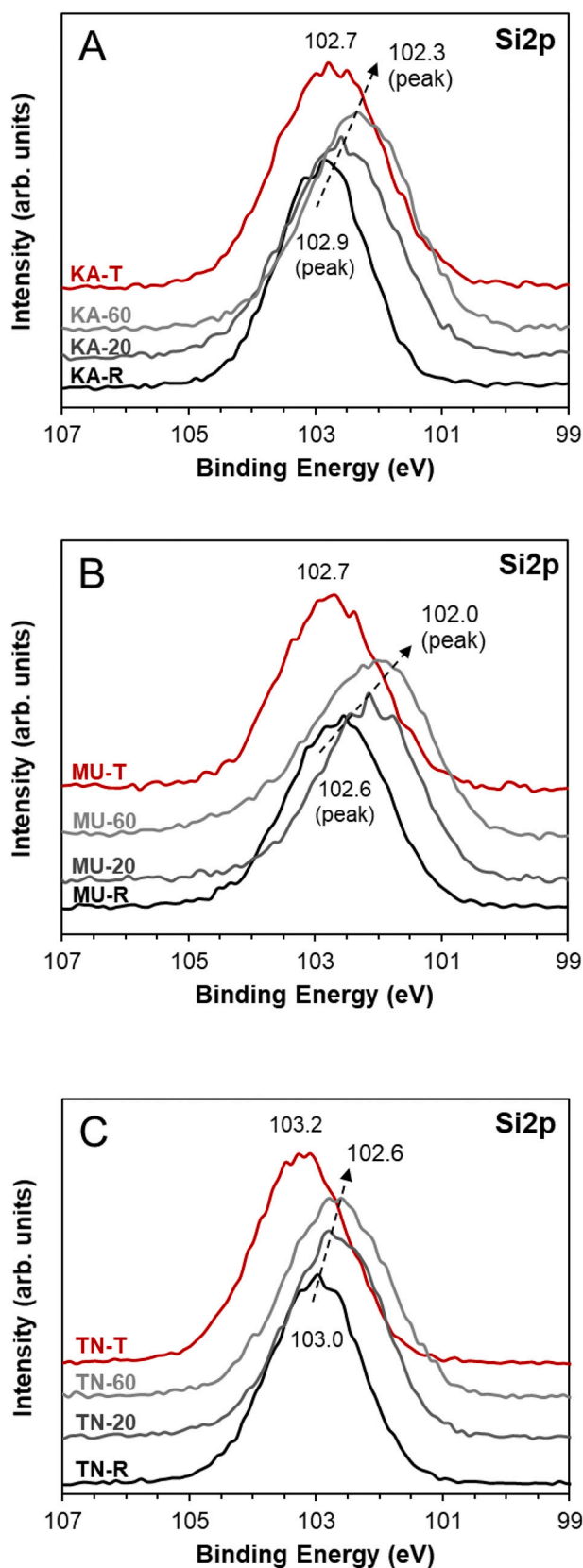

Fig. 7. XPS spectra of high resolution Al2p scan of (A) kaolinite, (B) muscovite, (C) montmorillonite. R-reference (as-received), 20-mechanochemically-activated for 20 min, 60-mechanochemically-activated for 60 min and T-thermally treated.

Fig. 8. XPS spectra of high resolution Si2p scan of (A) kaolinite, (B) muscovite, (C) montmorillonite. R-reference (as-received), 20-mechanochemically-activated for 20 min, 60-mechanochemically-activated for 60 min, T-thermally treated.

impact the Al2p binding energy. Compared with the as-received and thermally activated kaolin (KA-T), the symmetric Al2p spectrum broadened in peak width, and the peak centre shifted to a higher binding energy 74.9 eV. As for the as-received muscovite and montmorillonite mineral samples, they showed a symmetric peak centred at 74.4 eV and 74.7 eV, consistent with the values reported in the literature [65,66]. For both of these two types of minerals, mechanochemical activation led to significant decrease of Al2p binding energy from 0.3 to 0.4 eV for up to 60 min of activation. Along with the peak shift, a broadened spectra shape was also observed as the result of mechanochemical activation. On the other hand, thermal activation does not seem to affect the binding energy of Al2p in these two types of minerals. The broadening of the Al2p peaks is likely to be related to the amorphisation of the crystalline structure. The shift of the XPS Al2p peak reflects the change of the binding energy of the Al—O bonds on the surface layer (<10 nm) of the mineral samples investigated in this study. Since the binding energy is proportional to the dissolution (hydrolysation) rate of the same chemical bond [67], the decrease of the binding energy of the Al2p peak will likely result in a lower energy barrier for the Al—O bonds to be hydrolysed. This suggests that when used as SCMs, the mechanochemically treated muscovite and montmorillonite might be able to provide a higher level of Al source during the initial state of the pozzolanic reaction, compared with their thermally treated counterparts.

Fig. 8 summarised the XPS Si2p spectra of the three types of mineral samples assessed. The as-received kaolin, muscovite and montmorillonite showed symmetric Si2p peak centred at 102.9 eV, 102.6 eV, and 103.0 eV, consistent with that reported in literature [65,66]. The mechanochemical activation treatment led to consistent changes in the Si2p peak for all three minerals assessed, with the peak centre shifting to lower binding energy by 0.4 to 0.6 eV together with broadening of the peak shape. However, different performances were observed from samples after thermal treatment. The thermally treated kaolin showed much broader Si2p peak with the peak centre shifted to lower binding energy by 0.2 eV, while the peak centres of thermally treated muscovite and montmorillonite shifted to higher binding energy by 0.1 eV and 0.2 eV respectively. The broadening of the peak shape can also be observed from these two types of minerals after thermal activation. Similar to that observed from the Al2p spectra, the broaden of the Si2p peaks after either mechanochemical or thermal activations correspond to the amorphisation of the crystalline structures [68,69]. The Si2p peaks reflect the chemical environment of the Si—O—T(Si/Al) bonds on the surface of the assessed samples. In comparison with the Si—O—Si bond, the Si—O—Al bond possesses lower binding energy due to the increase of the negatively charge when Si is substituted by Al [70]. The shift of Si2p peaks to lower binding energy after the mechanochemical activation process relates to the decrease of binding energy of Si—O—T(Si/Al) bonds, which is likely caused by the increasing of Al substitution of the Si sites. The same surface aluminium enrichment phenomena have been reported for kaolin as the result of the mechanochemical activation process [45]. The results shown in Fig. 8 suggest that both the muscovite and montmorillonite minerals might have undergone similar surface aluminium enrichment process during the mechanochemical activation treatment. In addition, the decrease of binding energy of Si2p peak can also be attributed to the depolymerisation of silica species [68].

Table 4 summarised the surface Si/Al ratio as obtained from the XPS surface scans and the bulk Si/Al ratios of the as-received minerals determined by XRF analysis. The composition analysis has been performed according to the characteristic photoelectron line intensities after background removal, using the atomic sensitivity factors provided by the manufacturer. The results suggest that the surface Si/Al ratios of as-received minerals determined from the XPS results are consistent with the bulk Si/Al ratios determined from the XRF analysis. After thermal activation, the surface Si/Al ratios have not changed (only marginal differences). However, after mechanochemical activation, the surface Si/Al ratios decreased significantly, consistent with the

Atomic Si/Al ratios of as-received, thermally and mechanochemically activated minerals samples, as determined from XPS service scans (surface Si/Al) and XRF chemical compositions (bulk Si/Al).

	Surface Si/Al (determined from XPS)	Bulk Si/Al (determined from XRF)
KA-R	1.29	1.10
KA-T	1.31	–
KA-20	1.11	–
KA-60	1.08	–
MU-R	1.53	1.52
MU-T	1.56	–
MU-20	1.15	–
MU-60	1.19	–
TN-R	4.95	4.53
TN-T	4.97	–
TN-20	3.57	–
TN-60	3.46	–

observation of surface Al enrichment from the Si2p results. The decreases of the binding energy of both Si2p and Al2p spectra have also been observed from aluminosilicate zeolites with decreased Si/Al ratios [71], which also matches with the Si2p and Al2p spectra in this study. Since the Al—O bonds are more readily to be hydrolysed than the Si—O bonds [70], higher amount of Al will be supplied by the mechanochemically activated clays in comparison with thermally activated clays during the early stage of the reaction due to the preferential dissolution of Al. This also supports the hypothesis that mechanochemical activation might lead to better pozzolanic reactivity due to the modification of the chemical structure on the mineral surfaces, in addition to the dehydroxylation and amorphisation effects.

3.1.3. Bound water test for pozzolanic reactivity

Fig. 9 summarises the bound water percentages obtained according to the R^3 test, which is designed to assess the pozzolanic reactivity of supplementary cementitious materials. A higher percentage of bound water normally indicates higher pozzolanic reactivity and improved strength [72]. The R^3 test was used to assess the relative pozzolanic reactivity of the three minerals and the two different activation processes, as well as for selecting the optimal mechanochemical activator duration for further investigations. As indicated by the characterised
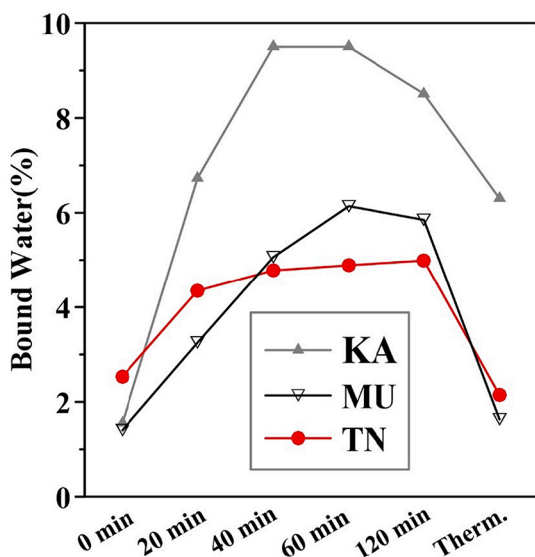
physical and chemical properties, the structural changes occurred during the mechanochemical activation treatment are likely to increase the pozzolanic activity of clay minerals. However, the correlations between the milling time and the resulted pozzolanic reactivities are still unclear.

The results shown in Fig. 9 suggest that, the bound water content of the mechanochemically activated clays increases as the milling time increases up to 60 min. Further increase of the milling time to 120 min led to decreased bound water content measured from the mechanochemically activated kaolin and muscovite. For montmorillonite, slight increases of the bound water content beyond 60 min of mechanochemical activation were observed. The bound water contents measured from the thermally treated samples are lower than all of the mechanochemically treated counterparts, suggesting that mechanochemical activation might be more efficient in improving the pozzolanic reactivity than the thermal activation method. Kaolin was the only thermally treated mineral that showed significantly increase of bound water content compared with the as-received mineral which confirms why metakaolin is commonly considered an effective pozzolanic material. The bound water content of the thermally treated kaolin characterised in this study resonates with the bound water capacity of calcined clay "CC2" reported in the RILEM TC 267-TRM phase 1and 2 [41,73]. The calcined clay "CC2" and the thermally treated kaolin clay from this study yield very similar amorphous content resulted from clay calcination (calculation processes can be found in the Supporting information). However, it is also worth to note that the newly revised procedure suggests preconditioning temperature of 40 °C instead of the 105 °C used in this study, which can result in higher characterised the bound water content (increase by around 60 %) for the same sample [73,74].

Based on the results shown in Fig. 9 and the characterisation results of mechanochemically activated samples, 60 min was chosen as the optimal mechanochemical activation condition and will be used for comparing the pozzolanic reactivities of mechanochemically or thermally treated samples in the following sections.

3.2. Performances as supplementary cementitious materials

3.2.1. Mineralogy of blended cement pastes

The phase assemblages (Fig. 10) and the thermogravimetry analysis (Fig. 11) of the blended cement pastes prepared with different mineral SCMs are analysed together to semi-quantitatively interpretate the phase assemblage changes in these binder systems. For interpretating the thermal analysis results, the mass loss below 120 °C is mainly attributed to the loss of water from the calcium (aluminate) silicate hydrate and ettringite, the mass loss between 120 °C and 200 °C is mainly attributed to the dehydration and dehydroxylation of the AFm phases, the mass loss between 400 °C and 500 °C is attributed to the dehydroxylation of portlandite, and the mass loss between 600 °C to 700 °C is attributed to the decarbonisation of carbonates (i.e. $CaCO_3$) [75,76].

The phase assemblages of the hydrate OPC paste (P-PC) are in line with that commonly reported in the literature [77], with a small fraction of unreacted clinker. Due to the presence of a small amount of $CaCO_3$ in the CEM I cement clinker (5.1 wt%), monocarbonate (PDF #00-036-0377) and hemicarbonate (PDF #00-036-0129) were formed instead of the monosulphate in the hydrate OPC paste (P-PC), suggesting that all of the sulphate ions might have been consumed by the ettringite phase [75]. As shown in Fig. 10, except for the unreacted as-received minerals (mainly as-received kaolin and muscovite), the replacement of 20 % of the cement clinker with clay minerals did not lead to new phases in the hydrated blended cement paste. The main differences between different mix designs lie in the changes of the relative intensities of portlandite, AFt and AFm phases. The unreacted as-received kaolin and muscovite (containing vermiculite) remained in the blended cement pastes, together with negligible changes in the relative intensities of portlandite comparing with the P-PC. This indicates the low pozzolanic reactivities of these two types of minerals, in accordance with that reported in the
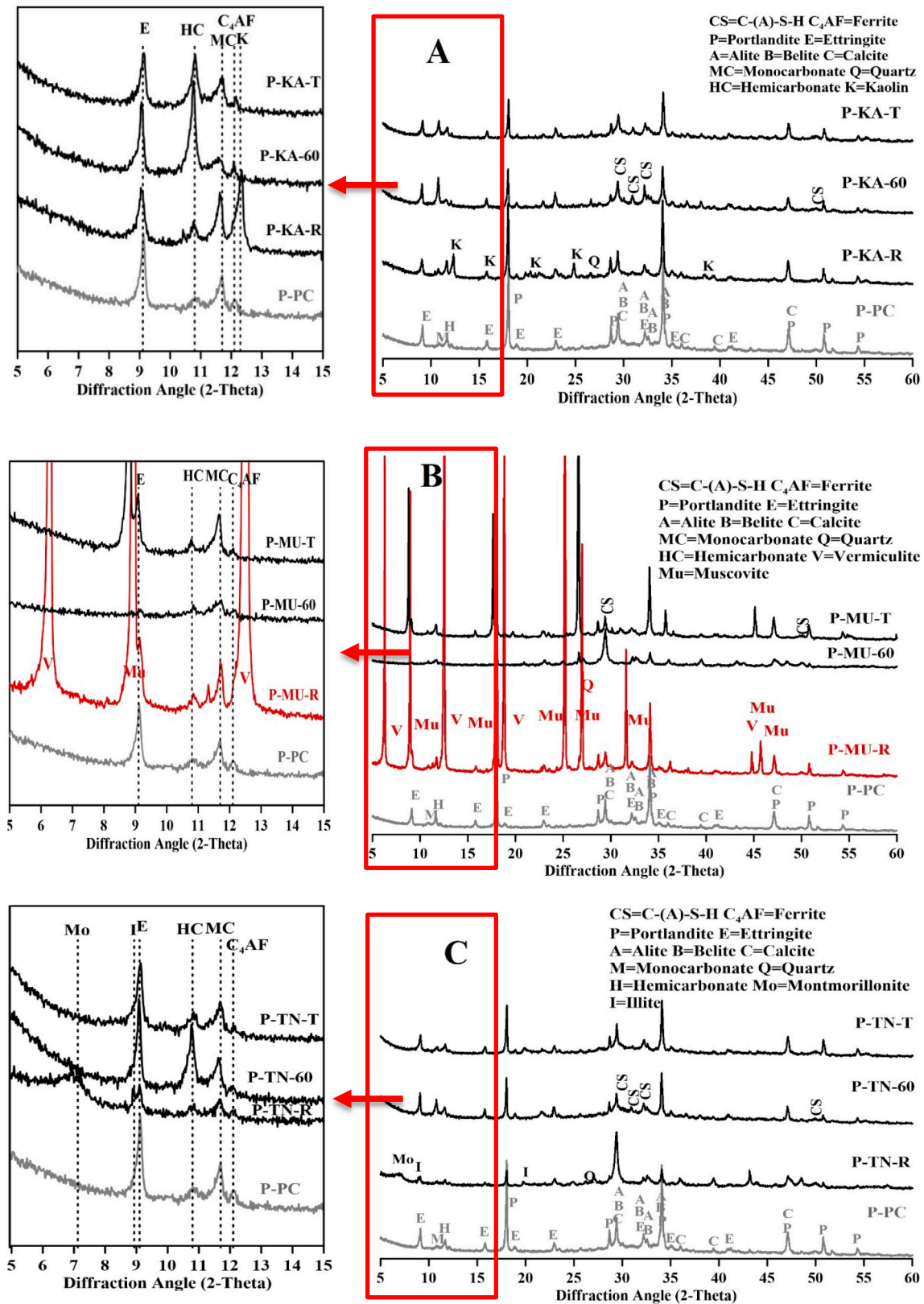

Fig. 9. The bound water test results according to R^3 test, where "0 min" corresponds to the as-received minerals and "Therm." refers to the thermally treated samples.

Fig. 10. XRD analysis of companion (P-PC), as-received (P-KA-R, P-MU-R and P-TN-R), mechanochemically activated and thermally activated kaolin (P-KA-60, P-MU-60 and P-TN-60), muscovite and montmorillonite blended system (P-KA-T, P-MU-T and P-TN-T).
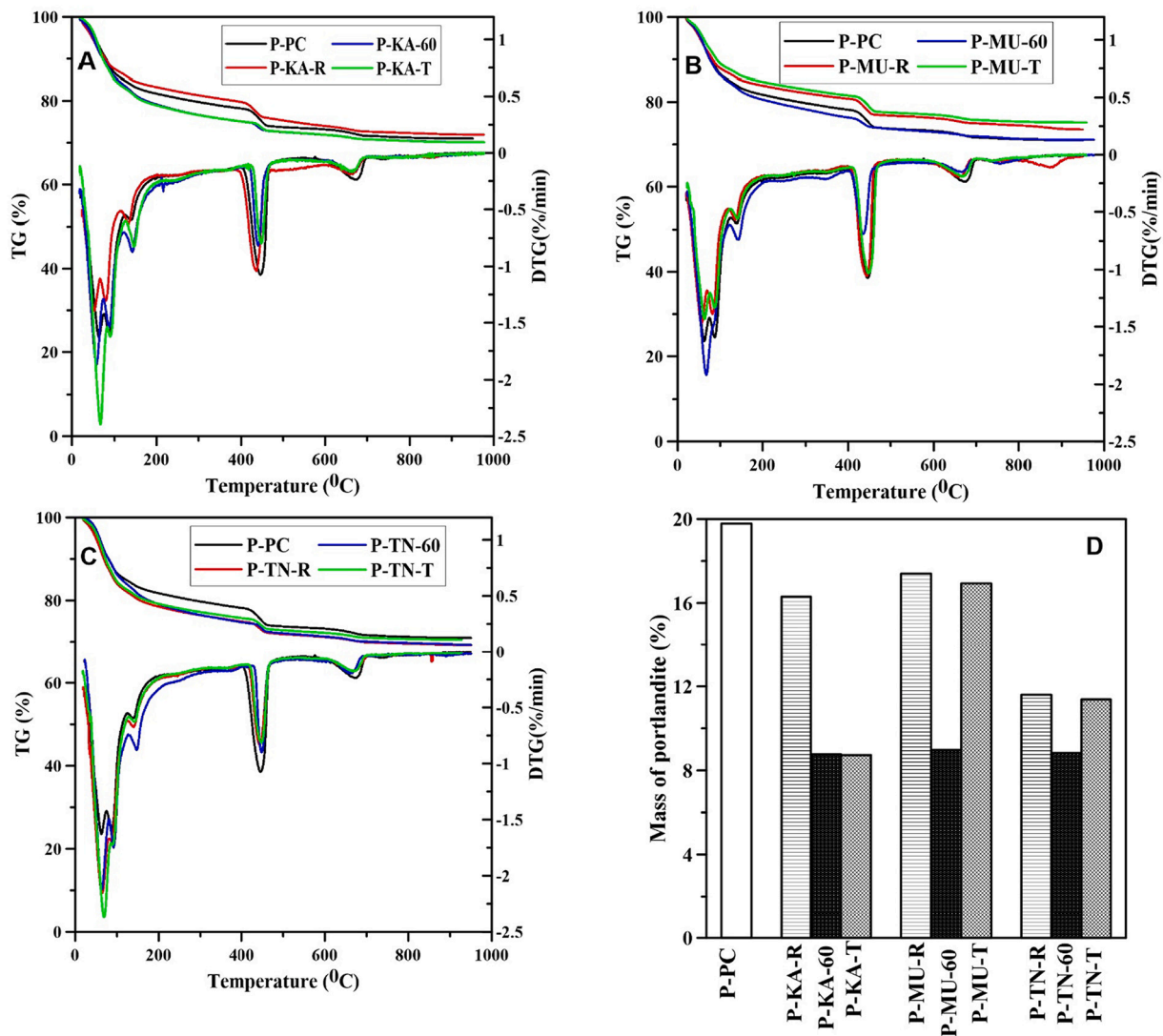
Fig. 11. TGA results and portlandite consumption of reference (P-PC), reference paste, as-received (P-KA-R, P-MU-R and P-TN-R), mechanochemically activated (P-KA-60, P-MU-60 and P-TN-60) and thermally activated (P-KA-T, P-MU-T and P-TN-T) kaolin, muscovite and montmorillonite blended system.

literature [34,78]. Only trace amounts of the montmorillonite were characterised from the sample using as-received montmorillonite as SCM (P-TN-R), where significant reduction in the relative intensities of portlandite was also observed. However, reflection peak matching the basal reflection of illite (as that observed from the thermally treated montmorillonite) was observed from the P-TN-R sample, suggesting the transiting of montmorillonite to illite is possibly due to selective consumption of Si or ion-exchange of interlayer cations [79].

Fig. 11D summarised the mass percentage of the portlandite in each of the blended samples as characterised from the thermal analysis. The thermal analysis results also suggest that as-received kaolin, muscovite and thermally treated muscovite have negligible pozzolanic reactivity (portlandite reduction mainly due to dilution effect with only 80 % PC addition). For samples prepared using mechanochemically treated minerals, significant reduction of portlandite can be observed, with around 50 % of the reduction even after taking into consideration of the dilution effect. Comparing with the thermally treated samples, mechanochemically treated muscovite showed the most significant portlandite reduction, followed by montmorillonite; however only marginal differences were observed from the kaolin samples after different treatments. The portlandite reduction is mainly attributed to the pozzolanic reaction between the supplementary cementitious materials and the portlandite, where a higher extent of reduction is often associated with a higher

degree of reaction of the supplementary cementitious materials [18]. It is also important to note that blended cement samples incorporating mechanochemical activated muscovite and montmorillonite consumed similar amount of portlandite when compared with thermally activated kaolin, suggesting similar portlandite consumption ability which might also indicate similar reactivity to thermally activated kaolin, which is one of the most reactive and well known supplementary cementitious materials.

The ettringite phase was significantly reduced from the mechanochemically activated muscovite (P-MU-60) and the as-received montmorillonite (P-TN-R). The reduction of ettringite might be due to reaction of ettringite with the Al provided by the reacted supplementary cementitious materials to form AFm phases [18,80]. This is consistent with the consumption of (activated) clay minerals and increased formation of carbonated AFm phases observed from this study. Increase of the relative content of hemicarbonate comparing to monocarbonate was observed from the thermally and mechanochemically activated kaolin, as well as the mechanochemically treated montmorillonite. This also suggests the formation of higher content of the total AFm phases due to significant consumption of Al provided by the treated clay mineral [81]. As the total carbonate source in the blended binder system is limited (only from the CEM I), the increase of the total AFm content can favor the formation of hemicarbonate over monocarbonate [82]. These

observations from XRD patterns are also supported by the thermal analysis (Fig. 11A, B and C), where higher mass loss between 120 °C and 200 °C were observed from these samples (particularly P-MU-60 and P-TN-60), indicating the presence of the higher amount of the total AFm phases. These results also correlates with the surface Al enrichment and

lower binding energy of Al—O and Si—O bonds in the mechanochemically treated samples, as suggested by the XPS results (Figs. 7 and 8).

3.2.2. Porosity and compressive strength

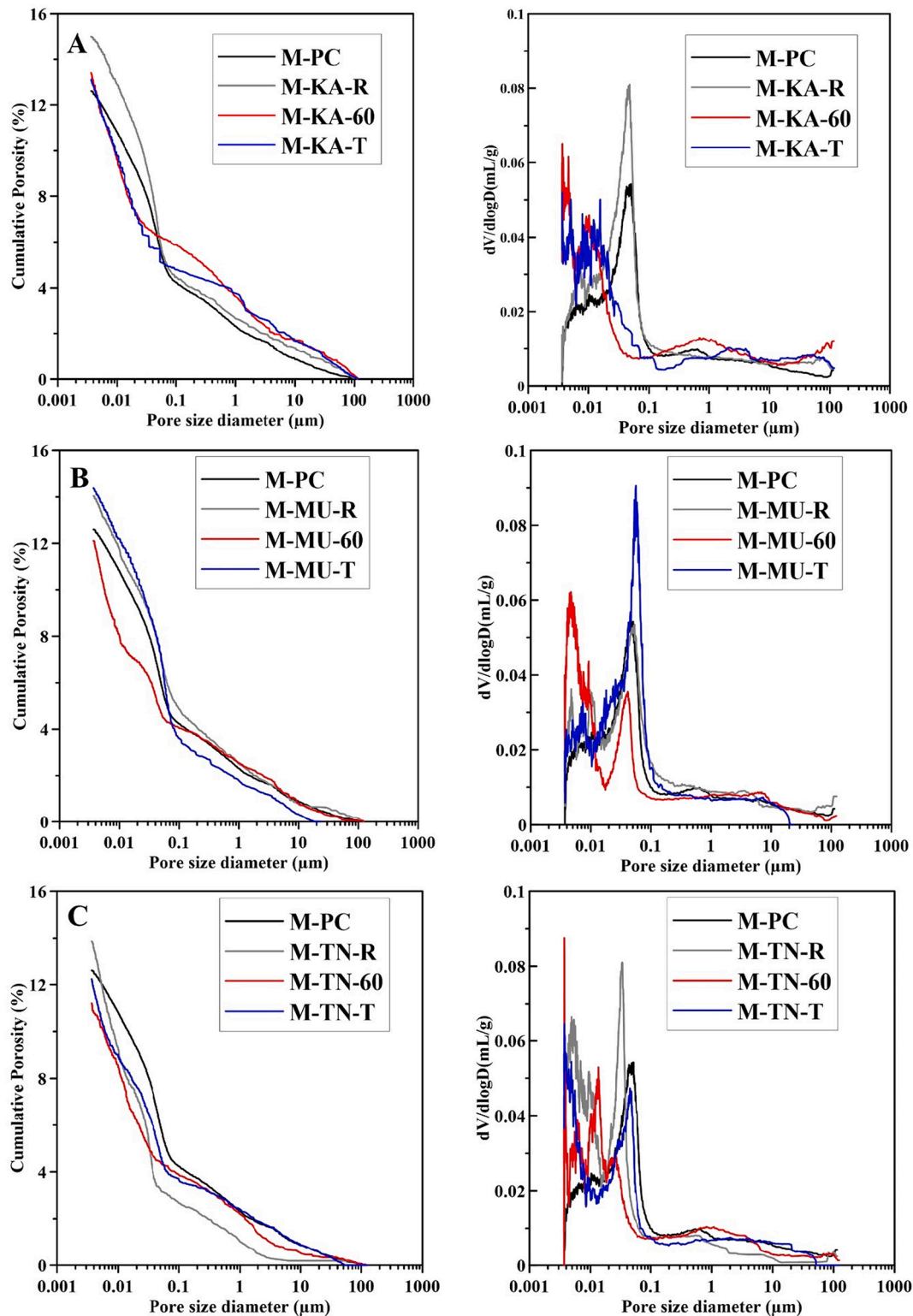Fig. 12 shows the cumulative porosity and pore size distribution of

Fig. 12. MIP cumulative porosity (left) and pore size distribution (right) results of standard CEM I mortar (M-PC) and blended cement mortars prepared using as-received ("-R") and treated ("-60" refers to "mechanochemical treated for 60 min", and "-T" refers to "thermally treated"), (A) kaolin, (B) muscovite and (C) montmorillonite as supplementary cementitious materials.

the standard CEM I mortar (M-PC) and the blended cement mortars at the age of 28 days as characterised by MIP. The standard CEM I mortar characterised in this study contains 79 % of capillary pores (10 nm to 10 μm) and 14 % of gel pores (<10 nm), consistent with that reported in the literature [7,83,84]. For mortar samples containing 20 % as-received kaolin or montmorillonite, higher percentages of both gel pores and capillary pores, as well as higher overall intrudable porosity, were observed in comparison to the standard CEM I mortar. These suggest coarsening of the microstructure in these blended mortars, most likely attributed by the formation of less hydration products due to low pozzolanic reactivities [7]. For mortars containing 20 % thermally treated kaolin, significant reduction of the capillary pores and increase of the gel pore were observed, where the use of mechanochemically treated kaolin further reduced the capillary pores and increased the gel pores. Similar trends were observed from the activated montmorillonite samples; however, the reduction in the capillary pore percentage was insignificant when thermally treated montmorillonite was used. The trend is slightly different for muscovite-related samples, where the placement of CEM I with the as received-muscovite led to slightly lower (marginal differences) porosity than that of the thermally treated muscovite. Both designs showed significantly higher total porosity than

that of the standard CEM I mortar, which is mainly attributed by the increased capillary pores content. But still, the sample prepared with mechanochemically treated muscovite showed a significant reduction in capillary pores together with the increase of gel pores.

The reduction of capillary pores and increase of gel pores in blended cement mortar are commonly associated with higher degree of pozzolanic reaction, which leads to densification of the microstructure and formation of more calcium (aluminium) silicate hydrates [7,85]. The results suggest that the mechanochemically treated clay minerals have the most significant effect on refining of the pore structure of the blended cement mortar at the current replacement level (20 %), similar to that reported in the literature [18]. The refined pore structures observed from these mortar samples suggest improved pozzolanic reactivity of the supplementary cementitious materials, which can be achieved by decreased particle size, increase specific surface areas, and/ or promoted surface dissolution [18,86]. As characterised in Section 3.1.1 (Figs. 1 and 3), the mechanochemically treated kaolin or mont-morillonite powder has similar particle size distribution and specific surface areas to that of their as-received and thermally treated coun-terparts. Therefore, the improved pozzolanic reactivity of the mecha-nochemical activated kaolin and montmorillonite might be primarily
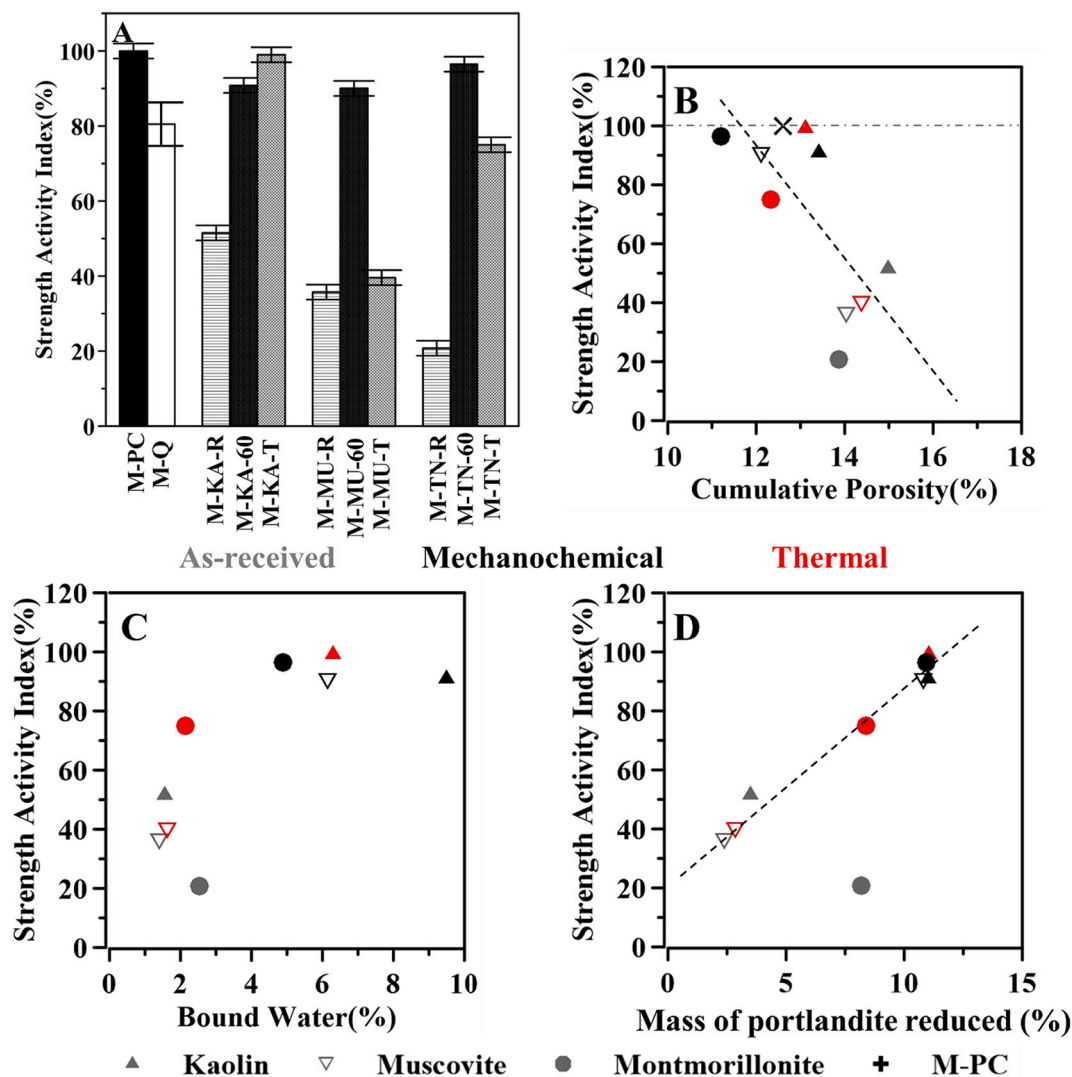

Fig. 13. (A) Compressive strength activity index (to the 28 days strength of cement mortar M-PC, 47.9 ± 1.9 MPa) of blended cement mortars replaced by different clay minerals, where "-R" refers to "as-received", "-60" refers to "mechanochemical treated for 60 min", and "-T" refers to "thermally treated". (B) Strength activity index versus cumulative porosity characterised from MIP; (C) strength activity index versus bound water content obtained using the R³ test methods; (D) strength activity index versus mass of portlandite reduced (portlandite in M-PC minus the remaining portlandite in blended cement) determined from TG analysis.

due to the surface Al enrichment and decreased binding energy of the Si—O and Al—O bond, both of which can promote the initial dissolution of the activated clay minerals [86]. However, the effect of reduced particle size and increased specific surface areas should be taken into consideration for the mechanochemically treated muscovite sample, considering the much larger particle size characterised from the as-received and thermally treated muscovite (Fig. 2).

The 28 days strength activity indexes (SAI) of the blended cement mortars were calculated according to the EN 196-1 standard [39]. The average 28 days strength of the standard CEM I mortar (M-PC, 47.9 ± 1.9 MPa) was used as the reference (100 % SAI), where the mortar prepared with 20 % fine quartz as inert SCM (representing the filler effect) has the average SAI value of 81 %. As shown in Fig. 13A, mechanochemical activation of kaolin, muscovite and montmorillonite by 60 min can achieve the SAI of around 90 % at the 20 % clinker replacement level, indicating good pozzolanic reactivity in addition to the filler effect. Except for the thermally activated kaolin, which achieved the highest strength, the mechanochemically activated clay minerals showed superior capacity in improving the strength performances of the blended mortar compared to the as-received and thermally treated clay minerals. Similar strength improvements have also been reported [9,31,34]. The thermally treated montmorillonite mostly acted as inert fillers, similar to that observed from literature where the montmorillonite were thermally activated at 600 °C and used in blended cement at the replacement level of 30 % [7]. However, since this study used relatively lower replacement level where the performances of inert and reactive SCM might be less significant [87], the thermally treated montmorillonite investigated in this study might also possess some pozzolanic reactivity in addition to the filler effect. The thermally activated kaolin (also known as metakaolin) is considered as one of the most commercially viable calcined clays, while 2:1 clays such as muscovite and montmorillonite are known to have low reactivity even after thermal treatment [7,34]. The results shown in this study suggest that mechanochemical activation of low reactivity 2:1 clays, like muscovite and montmorillonite, can effectively activate the original clay minerals to achieve similar strength performance in blended cement/mortar as the commonly used metakaolin.

Fig. 13B, C and D compared the SAI versus the MIP porosity, bound water content from R^3 test, and the reduced portlandite content (comparing to CEM I), respectively, which can help understand the main mechanisms that attribute to the desirable performances of mechanochemically activated clay minerals. Fig. 13B indicate that the strength performances are negatively correlated with their MIP porosity with close-to-linear correlations, suggesting that the blended mortar samples achieved higher strength possess denser microstructure, likely resulted from both promoted pozzolanic reaction and some filler effect [7,34]. Fig. 13C indicates that the SAI values are positively correlated to the bound water content from the R^3 test. Fig. 13D shows that, except for the as-received montmorillonite, the SAI values are positively correlated with the percentage of portlandite consumption in rigid linear correlations. These two plots (particularly Fig. 13D) confirm that samples with higher SAI are largely attributed to the improved pozzolanic reactivity of the activated clay minerals [77,88].

It is interesting to note that although mortars prepared from the as-received montmorillonite consumed the highest amount of portlandite comparing to kaolin and muscovite, it exhibited the lowest strength performances. The performances of this sample are also noticeably off from the major trends shown in Fig. 13B, C and D. Comparing with the thermally activated montmorillonite, the as-received montmorillonite showed similar capacity to react with the portlandite (Fig. 13C and D), but resulted in higher porosity (Fig. 13B) and much lower strength performances. As characterised by the XRD (Fig. 10C), the reaction between the as-received montmorillonite and portlandite resulted in formation of illite which does not contribute to the strength. The expansive nature of the as-received montmorillonite in the presence of water might attribute to the relative lower strength performances at the

same porosity content [15,77,89]. In addition, the agglomerating of montmorillonite particles can create big voids within the microstructure, the process of which can engage pozzolanic reactions but end up weakening the strength of the overall matrix [90].

In general, the bound water test results seem to show the least quantitative correlation with the strength performances at the SCM replacement level of 20 % (Fig. 13C), where a close to linear positive correlation might be expected [72]. The bound water content and the SAI of the thermally activated kaolin characterised in this study is consistent with that reported in [41] where the same bound water testing procedures were followed. The factors discussed above that interference with the pozzolanic reactivity of the as-received montmorillonite can also lead to higher bound water content. Besides, the bound water test results reported in literature are mostly based on calcined (thermally treated) kaolinite clay [72,74]. The unique surface properties and particle features (as shown in the Figs. 1–3) of the mechanochemical activated clays comparing to the thermally treated ones can affect both the early stage pozzolanic reactivity (of which the R^3 test represents [72]) and the long-term microstructure development (not reflected by the R^3 test). Particularly, since the bound water contents were measured at one given point, kinetic effect of the reaction cannot be reflected by the results [91]. The correlations between the bound water test results and the strength performances of cements blended with 2:1 clays or mechanochemically activated clays will need to be investigated in further details in future studies.

4. Conclusions

This research systematically assessed the impact of mechanochemical activation on the physicochemical properties of natural kaolinite, muscovite and montmorillonite minerals, and the influence of these properties on their pozzolanic activity when used as SCMs. The results show that mechanochemical activation can effectively promote the delamination, dehydroxylation and amorphisation of the original structures of kaolinite, muscovite (containing vermiculite) and montmorillonite within 60 min of high-impact milling (with the ball to clay mass ratio of 10/1 at the milling speed of 500 rpm). Extended milling does not necessarily lead to further decrease of particle sizes and can result in reduction of specific surface areas. The hydroxyl groups decomposed during the mechanochemical milling form water molecules absorbed onto the sample surface. In addition, surface aluminium enrichment was observed from all the mechanochemically treated samples resulting in the reduction of binding energies of the surface Al and Si elements (XPS results). Such surface aluminium enrichment phenomenon was not observed from the respective thermally treated samples.

At the 20 % replacement level, all of the mechanochemically treated clays investigated in this study achieved over 90 % of the strength activity index. For the 2:1 clays (muscovite, vermiculite, and montmorillonite), such performances are superior compared to the thermally treated and as-received counterparts; while for the 1:1 clay (kaolinite), the pozzolanic reactivity of mechanochemically treated kaolin was slightly lower than that of the thermally treated kaolin. Comparing the strength activity index with the bulk porosity, bound water content (R^3 test), and the portlandite reduction percentage, it seems that the superior strength performances of the mechanochemically activated 2:1 clays investigated in this study mainly result from the enhanced pozzolanic activity, and thus formation of higher amount of hydration products and densification of the microstructures. The surface aluminium enhancement effects of the mechanochemical mill process also played important roles in promoting the reaction of treated clays, leading to formation of higher amount of AFm phases.

This research has shown that mechanochemical activation treatment is particularly efficient for improving the pozzolanic activity of 2:1 clays (i.e. muscovite and montmorillonite), which are difficult to effectively activate through thermal treatments. The poor performance of these

minerals after thermal activation is a major reason why these abundant materials have not previously been extensively used as a cement replacement. This outcome therefore represents a step-change in developing new supplementary cementitious materials based on natural minerals which is timely considering the decreasing supplies of manufactured wastes and by-products such as fly as and ground granulated blastfurnace slag, and the increased importance of the reducing the environmental impact of concrete use. Nevertheless, the energy performances and cost-effectiveness of the mechanochemically activation method when scaling up from the lab scale to the commercial scale are still unknown. Case studies using commercial scale facilities or on-site equipment will be of great benefit to the future development of the mechanochemical activation method.

CRediT authorship contribution statement

Conceptualization, V. A. Baki and X. Ke; Funding acquisition, X. Ke and V. A. Baki; Investigation, V. A. Baki, X. Ke, A. Heath, J. Calabria-Holley; Methodology, V. A. Baki, X. Ke, A. Heath, J. Calabria-Holley; Project administration, V. A. Baki, X. Ke; Experimentation, V. A. Baki, C. Terzi, M. Sirin; Writing—original draft, V. A. Baki, X. Ke; Writing—review & editing, V. A. Baki, X. Ke, A. Heath, J. Calabria-Holley, C. Terzi, M. Sirin.

Declaration of competing interest

The authors declare that they have no known competing financial interests or personal relationships that could have appeared to influence the work reported in this paper.

Data availability

Data will be made available on request, and are also accessible through the University of Bath's research portal.

Appendix A. Supplementary data

Supplementary data to this article can be found online at https://doi.org/10.1016/j.cemconres.2022.106962.

References

[1] G. Habert, S.A. Miller, V.M. John, J.L. Provis, A. Favier, A. Horvath, K.L. Scrivener, Environmental impacts and decarbonization strategies in the cement and concrete industries, Nat. Rev. Earth Environ. 1 (2020) 559–573.

[2] P.J.M. Monteiro, S.A. Miller, A. Horvath, in: Towards Sustainable Concrete 16, 2017, pp. 698–699.

[3] IEA, Energy Technology Perspectives 2020, 2020.

[4] B. Bajzelj, J.M. Allwood, J.M. Cullen, in: Designing Climate Change Mitigation Plans That Add up 47, 2013, pp. 8062–8069.

[5] R.A. Robayo-Salazar, R.M. de Gutierrez, Natural volcanic pozzolans as an available raw material for alkali-activated materials in the foreseeable future: a review, Constr. Build. Mater. 189 (2018) 109–118.

[6] K.L. Scrivener, V.M. John, E.M. Gartner, U. Environment, Eco-efficient cements: potential economically viable solutions for a low-CO2 cement-based materials industry, Cem. Concr. Res. 114 (2018) 2–26.

[7] R. Fernandez, F. Martirena, K.L. Scrivener, The origin of the pozzolanic activity of calcined clay minerals: a comparison between kaolinite, illite and montmorillonite, Cem. Concr. Res. 41 (2011) 113–122.

[8] K. Scrivener, F. Martirena, S. Bishnoi, S. Maity, in: Calcined Clay Limestone Cements (LC3) 114, 2018, pp. 49–56.

[9] B. Ilić, V. Radonjanin, M. Malešev, M. Zdujić, A. Mitrović, in: Effects of Mechanical and Thermal Activation on Pozzolanic Activity of Kaolin Containing Mica 123, 2016, pp. 173–181.

[10] A.H. Ismail, A. Kusbiantoro, S.C. Chin, K. Muthusamy, M. Islam, K.F. Tee, Pozzolanic reactivity and strength activity index of mortar containing palm oil clinker pretreated with hydrochloric acid, J. Clean. Prod. 242 (2020), 118565.

[11] R.L. Frost, A.M. Vassallo, The dehydroxylation of the kaolinite clay minerals using infrared emission spectroscopy, clay, Clay Miner. 44 (1996) 635–651.

[12] R.Z. Rakhimov, N.R. Rakhimova, A.R. Gaifullin, V.P. Morozov, Properties of Portland cement pastes enriched with addition of calcined marl, J. Build Eng. 11 (2017) 30–36.

[13] S. Wild, J.M. Khatib, Portlandite consumption in metakaolin cement pastes and mortars, Cem. Concr. Res. 27 (1997) 137–146.

[14] M. Singh, M. Garg, Reactive pozzolana from indian clays - their use in cement mortars, Cement Concrete Res 36 (2006) 1903–1907.

[15] C.L. He, E. Makovicky, B. Osbaeck, Thermal stability and pozzolanic activity of raw and calcined mixed-layer mica/smectite, Appl. Clay Sci. 17 (2000) 141–161.

[16] R. Kumar, S. Kumar, S.P. Mehrotra, Towards sustainable solutions for fly ash through mechanical activation, Resour Conserv Recy 52 (2007) 157–179.

[17] D. Zhou, R. Wang, M. Tyrer, H. Wong, A.C. Cheeseman, Sustainable infrastructure development through use of calcined excavated waste clay as a supplementary cementitious material, J. Clean. Prod. 168 (2017) 1180–1192.

[18] A. Souri, H. Kazemi-Kamyab, R. Snellings, R. Naghizadeh, F. Golestani-Fard, K. Scrivener, Pozzolanic activity of mechanochemically and thermally activated kaolins in cement, Cement Concrete Res 77 (2015) 47–59.

[19] M. Fitos, E.G. Badogiannis, S.G. Tsivilis, M. Perraki, Pozzolanic activity of thermally and mechanically treated kaolins of hydrothermal origin, Appl. Clay Sci. 116 (2015) 182–192.

[20] E. Ivanov, C. Suryanarayana, Materials and process design through mechanochemical routes, J. Mater Synth. Process. 8 (2000) 235–244.

[21] X. Guo, D. Xiang, G. Duan, P. Mou, in: A review of mechanochemistry applications in waste management 30, 2010, pp. 4–10.

[22] P. Balaz, W. Choi, M. Fabian, E. Dutková, in: Mechanochemistry in the Preparation of Advanced Materials 11, 2006, pp. 122–129.

[23] V.V. Boldyrev, S.V. Pavlov, E.L. Goldberg, Interrelation between fine grinding and mechanical activation, Int. J. Miner. Process. 44–5 (1996) 181–185.

[24] G. Mucsi, S. Kumar, B. Csoke, R. Kumar, Z. Molnar, A. Racz, F. Madai, A. Debreczeni, Control of geopolymer properties by grinding of land filled fly ash, Int. J. Miner. Process. 143 (2015) 50–58.

[25] G. Kaupp, Mechanochemistry: the varied applications of mechanical bond-breaking, CrystEngComm 11 (2009) 388–403.

[26] F. Matalkah, L. Xu, W. Wu, P. Soroushian, in: Mechanochemical Synthesis of One-part Alkali Aluminosilicate Hydraulic Cement 50, 2016, p. 97.

[27] M. Wahl, U. Brocke, L. Brendel, H.J. Feise, B. Weigl, M. Rock, J. Schwedes, Understanding powder caking: predicting caking strength from individual particle contacts, Powder Technol. 188 (2008) 147–152.

[28] F.K.h. Urakaev, Mechanism and kinetics of mechanochemical processes, in: M. Sopicka-Lizer (Ed.), High-Energy Ball Milling, Woodhead Publishing, 2010, pp. 9–44.

[29] P. Ciccioli, D. Capitani, S. Gualtieri, E. Soragni, G. Belardi, P. Plescia, G. Contini, Mechano-chemistry of rock materials for the industrial production of new geopolymeric cements, in: Factories of the Future, 2019, pp. 383–407.

[30] A.M. Rashad, Metakaolin as cementitious material: history, scours, production and composition - a comprehensive overview, Constr. Build. Mater. 41 (2013) 303–318.

[31] C. Vizcayno, R.M. de Gutierrez, R. Castello, E. Rodriguez, C.E. Guerrero, Pozzolan obtained by mechanochemical and thermal treatments of kaolin, Appl. Clay Sci. 49 (2010) 405–413.

[32] G. Yao, T. Cui, Z. Jia, S.K. Sun, C. Anning, J. Qiu, X.J. Lyu, Effect of anhydrite on hydration properties of mechanically activated muscovite in the presence of calcium oxide, Appl. Clay Sci. 196 (2020), 105742.

[33] E.F. Aglietti, J.M.Porto Lopez, E. Pereira, in: Mechanochemical Effects in Kaolinite Grinding. I. Textural and Physicochemical Aspects 16, 1986, pp. 125–133.

[34] G. Yao, H.Y. Zang, J.X. Wang, P. Wu, J. Qiu, X.J. Lyu, Effect of mechanical activation on the pozzolanic activity of muscovite, clay, Clay Miner. 67 (2019) 209–216.

[35] I. Tole, K. Habermehl-Cwirzen, M. Rajczakowska, A. Cwirzen, Activation of a Raw Clay by Mechanochemical Process-Effects of Various Parameters on the Process Efficiency and Cementitious Properties 11, 2018.

[36] S. Hollanders, R. Adriaens, J. Skibsted, O. Cizer, J. Elsen, Pozzolanic reactivity of pure calcined clays, Appl. Clay Sci. 132 (2016) 552–560.

[37] E. Badogiannis, G. Kakali, S. Tsivilis, Metakaolin as supplementary cementitious material - optimization of kaolin to metakaolin conversion, J. Therm. Anal. Calorim. 81 (2005) 457–462.

[38] A. Chakchouk, L. Trifi, B. Samet, S. Bouaziz, Formulation of blended cement: effect of process variables on clay pozzolanic activity, Constr. Build. Mater. 23 (2009) 1365–1373.

[39] BS EN 196-1:2016, Methods of testing cement, in: Determination of Strength, British Standards Institute, 2016.

[40] A. International, Standard Test Methods for Measuring the Reactivity of Supplementary Cementitious Materials by Isothermal Calorimetry and Bound Water Measurements, ASTM C1897-20, ASTM, West Conshohocken, PA, 2020.

[41] X.R. Li, R. Snellings, M. Antoni, N.M. Alderete, M. Ben Haha, S. Bishnoi, O. Cizer, M. Cyr, K. De Weerdt, Y. Dhandapani, J. Duchesne, J. Haufe, D. Hooton, M. Juenger, S. Kamali-Bernard, S. Kramar, M. Marroccoli, A.M. Joseph, A. Parashar, C. Patapy, J.L. Provis, S. Sabio, M. Santhanam, L. Steger, T.B. Sui, A. Telesca, A. Vollpracht, F. Vargas, B. Walkley, F. Winnefeld, G. Ye, M. Zajac, S. Z. Zhang, K.L. Scrivener, Reactivity tests for supplementary cementitious materials: RILEM TC 267-TRM phase 1, Mater. Struct. 51 (2018) 151.

[42] I. Tole, K. Habermehl-Cwirzen, A. Cwirzen, Mechanochemical activation of natural clay minerals: an alternative to produce sustainable cementitious binders - review, Miner Petrol 113 (2019) 449–462.

[43] P.J. Sánchez-Soto, M.Carmen Jiménez de Haro, L.A. Pérez-Maqueda, I. Varona, J. L. Pérez-Rodríguez, in: Effects of Dry Grinding on the Structural Changes of Kaolinite Powders 83, 2004, pp. 1649–1657.

[44] L. Andrić, A. Terzić, Z. Aćimović-Pavlović, L. Pavlović, M. Petrov, in: Comparative Kinetic Study of Mechanical Activation Process of Mica and Talc for Industrial Application 59, 2014, pp. 181–190.

[45] A. Mitrović, M. Zdujić, in: Preparation of Pozzolanic Addition by Mechanical Treatment of Kaolin Clay 132, 2014, pp. 59–66.

[46] G. Suraj, C.S.P. Iyer, S. Rugmini, M. Lalithambika, The effect of micronization on kaolinites and their sorption behaviour, Appl. Clay Sci. 12 (1997) 111–130.

[47] É. Kristóf, in: The Effect of Mechanical Treatment on the Crystal Structure and Thermal Behavior of Kaolinite 41, 1993, pp. 608–612.

[48] H. Yanguatin, J.H. Ramirez, A. Tironi, J.I. Tobon, Effect of thermal treatment on pozzolanic activity of excavated waste clays, Constr. Build. Mater. 211 (2019) 814–823.

[49] F. Dellisanti, G. Valdre, Study of structural properties of ion treated and mechanically deformed commercial bentonite, Appl. Clay Sci. 28 (2005) 233–244.

[50] N. Vdović, I. Jurina, S.D. Škapin, I. Sondi, in: The Surface Properties of Clay Minerals Modified by Intensive Dry Milling — Revisited 48, 2010, pp. 575–580.

[51] I. Sondi, M. Stubicar, V. Pravdic, Surface properties of ripidolite and beidellite clays modified by high-energy ball milling, Colloids Surf. A 127 (1997) 141–149.

[52] M. Valásková, J. Madejová, A. Inayat, L. Matějová, M. Ritz, A. Martaus, P. Leštinský, Vermiculites From Brazil and Palabora: Structural Changes Upon Heat Treatment and Influence on the Depolymerization of Polystyrene 192, 2020.

[53] S.C. Taylor-Lange, E.L. Lamon, K.A. Riding, M.C.G. Juenger, Calcined kaolinite-bentonite clay blends as supplementary cementitious materials, Appl. Clay Sci. 108 (2015) 84–93.

[54] V.S. Fajnor, K. Jesenak, Differential thermal analysis of montmorillonite, J. Therm. Anal. Calorim. 46 (1996) 489–493.

[55] J.Y. Tang, Y.M. Zhang, S.X. Bao, The influence of roasting temperature on the flotation properties of muscovite, Minerals-Basel 6 (2016).

[56] C.L. He, E. Makovicky, B. Osbaeck, Thermal treatment and pozzolanic activity of Na- and Ca-montmorillonite, Appl. Clay Sci. 10 (1996) 351–368.

[57] É. Makó, R.L. Frost, J. Kristóf, E. Horváth, in: The Effect of Quartz Content on the Mechanochemical Activation of Kaolinite 244, 2001, pp. 359–364.

[58] O. Juhász, Mechanical activation of minerals by grinding pulverizing and morphology of particles, in: Acta Mineralogica-Petrographica, Proceedings of the 10th International Kaolin Symposium Budapest, 1980.

[59] V.M. Malhotra, A.A. Ogloza, Ftir spectra of hydroxyls and dehydroxylation kinetics mechanism in montmorillonite, Phys. Chem. Miner. 16 (1989) 386–393.

[60] M. Janek, I. Bugar, D. Lorenc, V. Szocs, D. Velic, D. Chorvat, Terahertz time-domain spectroscopy of selected layered silicates, clay, Clay Miner. 57 (2009) 416–424.

[61] J. Hrachova, J. Madejova, P. Billik, P. Komadel, V.S. Fajnor, in: Dry Grinding of Ca and Octadecyltrimethylammonium Montmorillonite 316, 2007, pp. 589–595.

[62] J.G. Miller, T.D. Oulton, Prototropy in kaolinite during percussive grinding, clay, Clay Miner. 18 (1970) 313-+.

[63] J.-F. Lambert, W.S. Millman, J.J. Fripiat, in: Revisiting Kaolinite Dehydroxylation: A Silicon-29 and Aluminum-27 MAS NMR Study 111, 1989, pp. 3517–3522.

[64] U.B. Gunatilake, J. Bandara, in: Fabrication of Highly Hydrophilic Filter Using Natural and Hydrothermally Treated Mica Nanoparticles for Efficient Waste Oil-Water Separation 191, 2017, pp. 96–104.

[65] R.M. Torres Sanchez, E.I. Basaldella, J.F. Marco, The effect of thermal and mechanical treatments on kaolinite, in: Characterization by XPS and IEP Measurements 215, 1999, pp. 339–344.

[66] J.T. Kloprogge, B.J. Wood, Phyllo-silicates, handbook of mineral, Spectroscopy (2020) 359–429.

[67] M. Najib, R.B. Hammond, T. Mahmud, T. Izumi, Impact of structural binding energies on dissolution rates for single faceted-crystals, Cryst. Growth Des. 21 (2021) 1482–1495.

[68] L. Black, K. Garbev, G. Beuchle, P. Stemmermann, D. Schild, X-ray photoelectron spectroscopic investigation of nanocrystalline calcium silicate hydrates synthesised by reactive milling, Cem. Concr. Res 36 (2006) 1023–1031.

[69] I. Garcia-Lodeiro, A. Fernández-Jimenez, A. Palomo, in: Cements With a Low Clinker Content: Versatile Use of Raw Materials 4, 2015, pp. 140–151.

[70] H. Seyama, K. Kinoshita, M. Soma, Surface alteration of plagioclase during acid dissolution, Surf. Interface Anal. 34 (2002) 289–292.

[71] I. Jirka, Initial and final state effects in the photoelectron and auger spectra of Si and Al bonded in zeolites, J. Phys. Chem. B 101 (1997) 8133–8140.

[72] F. Avet, R. Snellings, A. Alujas Diaz, M. Ben Haha, K. Scrivener, in: Development of a new rapid, relevant and reliable (R3) test method to evaluate the pozzolanic reactivity of calcined kaolinitic clays 85, 2016, pp. 1–11.

[73] F. Avet, X. Li, M. Ben Haha, S.A. Bernal, S. Bishnoi, Ö. Cizer, M. Cyr, S. Dolenec, P. Durdzinski, J. Haufe, D. Hooton, M.C.G. Juenger, S. Kamali-Bernard, D. Londono-Zuluaga, A.T.M. Marsh, M. Marroccoli, M. Mrak, A. Parashar, C. Patapy, M. Pedersen, J.L. Provis, S. Sabio, S. Schulze, R. Snellings, A. Telesca, M. Thomas, F. Vargas, A. Vollpracht, B. Walkley, F. Winnefeld, G. Ye, S. Zhang, K. Scrivener, Report of RILEM TC 267-TRM phase 2: optimization and testing of the robustness of the R3 reactivity tests for supplementary cementitious materials, Mater. Struct. 55 (2022) 92.

[74] D. Londono-Zuluaga, A. Gholizadeh-Vayghan, F. Winnefeld, F. Avet, M. Ben Haha, S.A. Bernal, Ö. Cizer, M. Cyr, S. Dolenec, P. Durdzinski, J. Haufe, D. Hooton, S. Kamali-Bernard, X. Li, A.T.M. Marsh, M. Marroccoli, M. Mrak, C. Patapy, M. Pedersen, S. Sabio, S. Schulze, R. Snellings, A. Telesca, A. Vollpracht, G. Ye, S. Zhang, K.L. Scrivener, in: Report of RILEM TC 267-TRM Phase 3: Validation of the R3 Reactivity Test Across a Wide Range of Materials 55, 2022, p. 142.

[75] B. Lothenbach, G. Le Saout, E. Gallucci, K. Scrivener, Influence of limestone on the hydration of Portland cements, Cement Concrete Res 38 (2008) 848–860.

[76] J. Dweck, P.M. Buchler, A.C.V. Coelho, F.K. Cartledge, Hydration of a Portland cement blended with calcium carbonate, Thermochim. Acta 346 (2000) 105–113.

[77] S. Khandelwal, K.Y. Rhee, Evaluation of pozzolanic activity, heterogeneous nucleation, and microstructure of cement composites with modified bentonite clays, Constr. Build. Mater. 323 (2022), 126617.

[78] Y.Y. Liu, S.M. Lei, M. Lin, Y. Li, Z. Ye, Y.M. Fan, Assessment of pozzolanic activity of calcined coal-series kaolin, Appl. Clay Sci. 143 (2017) 159–167.

[79] D. Savage, J. Wilson, S. Benbow, H. Sasamoto, C. Oda, C. Walker, D. Kawama, Y. Tachi, Natural systems evidence for the effects of temperature and the activity of aqueous silica upon montmorillonite stability in clay barriers for the disposal of radioactive wastes, Appl. Clay Sci. 179 (2019), 105146.

[80] K. De Weerdt, M.B. Haha, G. Le Saout, K.O. Kjellsen, H. Justnes, B. Lothenbach, in: Hydration Mechanisms of Ternary Portland Cements Containing Limestone Powder and Fly Ash 41, 2011, pp. 279–291.

[81] J. Skibsted, R. Snellings, Reactivity of supplementary cementitious materials (SCMs) in cement blends, Cem. Concr. Res. 124 (2019), 105799.

[82] Q.Y. Shao, K.R. Zheng, X.J. Zhou, J. Zhou, X.H. Zeng, Enhancement of nano-alumina on long-term strength of Portland cement and the relation to its influences on compositional and microstructural aspects, Cement Concrete Comp 98 (2019) 39–48.

[83] J. Ren, X. Luo, R. Bai, C. Pan, J. Zhang, in: Pore Characteristics of Different Phase in Nano-modified Concrete and Their Influences on the Compressive Strength 46, 2022, p. 103784.

[84] E. Janowska-Renkas, J. Kowalska, G. Janus, A. Kaliciak, Cement-fly ash mortars durability, with fly ash from fluidized bed boilers and conventional combustion, exposed to aggressive environment influence, Matec Web Conf 174 (2018) 02006.

[85] S.K. Cheng, K.Y. Ge, T. Sun, Z.H. Shui, X.Y. Chen, J.X. Lu, Pozzolanic activity of mechanochemically and thermally activated coal-series kaolin in cement-based materials, Constr. Build. Mater. 299 (2021), 123972.

[86] H. Niu, P. Kinnunen, H. Sreenivasan, E. Adesanya, M. Illikainen, Structural collapse in phlogopite mica-rich mine tailings induced by mechanochemical treatment and implications to alkali activation potential, Miner. Eng. 151 (2020), 106331.

[87] S. Ramanathan, M. Croly, P. Suraneni, Comparison of the effects that supplementary cementitious materials replacement levels have on cementitious paste properties, Cem. Concr. Compos. 112 (2020), 103678.

[88] G. Yao, T. Cui, J.K. Zhang, J.X. Wang, X.J. Lyu, Effects of mechanical grinding on pozzolanic activity and hydration properties of quartz, Adv. Powder Technol. 31 (2020) 4500–4509.

[89] J.P. Du, A.N. Zhou, X.S. Lin, Y.H. Bu, J. Kodikara, Revealing expansion mechanism of cement-stabilized expansive soil with different interlayer cations through molecular dynamics simulations, J. Phys. Chem. C 124 (2020) 14672–14684.

[90] J. Calabria-Holley, S. Papatzani, B. Naden, J. Mitchels, K. Paine, Tailored montmorillonite nanoparticles and their behaviour in the alkaline cement environment, Appl. Clay Sci. 143 (2017) 67–75.

[91] S. Ramanathan, L.R. Pestana, P. Suraneni, Reaction kinetics of supplementary cementitious materials in reactivity tests, Cement 8 (2022), 100022.